Characteristics of Vertical Air Motion in Isolated Convective Clouds

Jing Yang[1], Zhien Wang[1], Andrew J. Heymsfield[2] and Jeffrey R. French[1]

[1] {Department of Atmospheric Science, University of Wyoming, Laramie, WY}

[2] {National Center for Atmospheric Research, Boulder, CO}

Correspondence to: Zhien Wang (zwang@uwyo.edu)

Abstract

The vertical velocity and air mass flux in isolated convective clouds are statistically analyzed using aircraft in-situ data collected from three field campaigns: High-Plains Cumulus (HiCu) conducted over the mid-latitude High Plains, COnvective Precipitation Experiment (COPE) conducted in a mid-latitude coastal area, and Ice in Clouds Experiment-Tropical (ICE-T) conducted over a tropical ocean. The results show small-scale updrafts and downdrafts (< 500 m in diameter) are frequently observed in the three field campaigns, and they make important contributions to the total air mass flux. The probability density functions (PDFs) and profiles of the observed vertical velocity are provided. The PDFs are exponentially distributed. The updrafts generally strengthen with height. Relatively strong updrafts (> 20 m s^{-1}) were sampled in COPE and ICE-T. The observed downdrafts are stronger in HiCu and COPE than in ICE-T. The PDFs

of the air mass flux are exponentially distributed as well. The observed maximum air mass flux in updrafts is of the order 10^4 kg m^{-1} s^{-1}. The observed air mass flux in the downdrafts is typically a few times smaller in magnitude than that in the updrafts. Since this study only deals with isolated convective clouds, and there are many limitations and sampling issues in aircraft in-situ measurements, more observations are needed to better explore the vertical air motion in convective clouds.

1. Introduction

Convective clouds are an important component of the global energy balance and water cycle because they dynamically couple the planetary boundary layer to the free troposphere through the vertical transport of heat, moisture and mass (Arakawa, 2004; Heymsfield et al., 2010; Wang and Geerts, 2013). The vertical velocity determines the vertical transport of cloud condensate, the cloud top height, and the detrainment into anvils, which further influences the radiative balance (Del Genio et al., 2005). Vertical velocity also has a significant impact on aerosol activation, droplet condensation and ice nucleation in convective clouds, which in turn impacts cloud life cycle and precipitation efficiency.

In order to reasonably simulate convective clouds, the vertical air velocity must be parameterized reliably in numerical weather prediction models (NWPMs) and global circulation models (GCMs) (Donner et al., 2001; Tonttila et al., 2011; Wang and Zhang, 2014). However, the complexity of the vertical velocity structure in convective clouds makes the parameterization non-straightforward (Wang and Zhang, 2014). Observations show that in most of convective clouds the vertical velocity is highly variable, and consequently the detailed structure of convection

cannot be resolved in many models (Kollias et al., 2001; Tonttila et al., 2011). Additionally, using the same parameterization of vertical velocity for different grid resolutions may result in different cloud and precipitation properties (Khairoutdinov et al., 2009). Furthermore, poorly parameterized vertical velocity may result in large uncertainties in the microphysics; for instance, the cloud droplet concentration may be underestimated due to unresolved vertical velocity (Ivanova and Leighton, 2008). Vertical velocity simulated by models with horizontal resolutions of a few hundred meters may be more realistic (e.g. Wu et al., 2009), but more observations are needed to evaluate this suggestion.

Aircraft in-situ measurement has been the most reliable tool enabling us to understand the vertical velocity in convective clouds and to develop the parameterizations for models. Early studies (e.g. Byers and Braham, 1949; Schmeter, 1969) observed strong updrafts and downdrafts in convective clouds, however, their results have large uncertainties, because the aircrafts were not equipped with inertial navigation systems (LeMone and Zipser, 1980). In 1974, the Global Atmospheric Research Program (GARP) Atlantic Tropical Experiment (GATE) was conducted off the west coast of Africa, focusing on tropical maritime convections (Houze, 1981). A series of findings based on the aircraft data collected from the project were reported. For example, the accumulated probability density functions (PDFs) of vertical velocity and diameter of the convective cores are lognormally distributed. The updrafts and downdrafts in GATE (tropical maritime clouds) were only one half to one third as strong as those observed in the Thunderstorm Project (continental clouds) (LeMone and Zipser, 1980; Houze, 1981). These findings stimulated later statistical studies of the vertical velocity in convective clouds. Jorgensen et al. (1985) found that the accumulated PDFs of vertical velocity in intense hurricanes were also distributed lognormally and the strength was similar to that in GATE, but the diameter of the convective

region was larger. Studies of convective clouds over Taiwan (Jorgensen and LeMone, 1989) and Australia (Lucas et al., 1994) showed a magnitude of vertical velocity similar to that in GATE. Although the results from the Thunderstorm Project are suspect, the significantly stronger drafts reveal the possible difference between continental and tropical maritime convective clouds. Lucas et al. (1994) suggested that water loading and entrainment strongly reduce the strength of updrafts in maritime convection. However, this underestimation of the updraft intensity may be also due to sampling issues, e.g. penetrations were made outside the strongest cores (Heymsfield et al., 2010).

There are a few more recent aircraft measurements (e.g. Igau et al, 1999; Anderson et al., 2005), but the data are still inadequate to fully characterize the vertical velocity in convective clouds. In most of these earlier papers, the defined draft or draft core required a diameter no smaller than 500 m; this threshold excluded many narrow drafts with strong vertical velocity and air mass flux. In addition, the earlier studies used 1-Hz resolution data, which, at typical aircraft flight speeds, can resolve only vertical velocity structures larger than a few hundred meters, but the narrow drafts may be important to the total air mass flux exchange and cloud evolution. Furthermore, previous aircraft observations for continental convective clouds were based only on the Thunderstorm Project, thus, additional data are needed to study the difference between continental and maritime convections.

Remote sensing by means of, for example, wind profiling radars is another technique that has often been used in recent years for studying the vertical velocity in convective clouds (e.g. Kollias et al., 2001; Hogan et al., 2009; Giangrande et al., 2013; Schumacher et al., 2015). Using profiler data, May and Rajopadhyaya (1999) analyzed the vertical velocity in deep convections near Darwin, Australia. They observed that the updraft intensified with height and that the

maximum vertical velocity was greater than 15 m s^{-1}. Heymsfield et al. (2010) studied the vertical velocity in deep convection using an airborne nadir-viewing radar. Strong updrafts were observed over both continental and ocean areas, with the peak vertical velocity exceeding 15 m s^{-1} in most of the cases and exceeding 30 m s^{-1} in a few cases. Zipser et al. (2006) used satellite measurements to find the most intense thunderstorms around the world; they applied a threshold updraft velocity greater than 25 m s^{-1} to identify intense convection. Collis et al. (2013) provided statistics of updraft velocities for different convective cases near Darwin, Australia using retrievals from scanning Doppler radars and a multi-frequency profiler. Airborne volumetric Doppler radars have also been used to study the dynamic structure of convective clouds (e.g. Jorgensen and Smull 1993; Hildebrand et al. 1996; Jorgensen et al. 2000). Remote sensing has the advantage of being able to measure the vertical velocity at different heights simultaneously (Tonttila et al., 2011), and some of the techniques can detect the strongest updraft cores in convective clouds (Heymsfield et al. 2010; Collis et al. 2013). Volumetric radars can also provide three-dimensional (3D) structure of air motion in convective clouds (Collis et al. 2013; Nicol et al. 2015; Jorgensen et al. 2000). However, remote sensing measurements are not as accurate as aircraft measurements, because of the assumptions needed to account for the contribution of hydrometeor fall speed in the observed Doppler velocity in order to ultimately estimate air velocity. In addition, ground-based radars can rarely provide good measurements over oceans, and airborne cloud radars often suffer from the attenuation and non-Rayleigh scattering in convective clouds. Therefore, in-situ measurements are still necessary in order to characterize the dynamics in convective clouds and to develop parameterizations for models.

The present study provides aircraft data analysis of updrafts and downdrafts in mid-latitude continental, mid-latitude coastal, and tropical maritime convective clouds using the fast-response

in-situ measurements collected from three field campaigns: the High-Plains Cumulus (HiCu) project, the COnvective Precipitation Experiment (COPE) and the Ice in Clouds Experiment-Tropical (ICE-T). All data used in this study were compiled for individual, isolated penetrations. Statistics of the vertical velocity and air mass flux are provided. The Wyoming Cloud Radar (WCR), onboard the aircraft, is used to identify the cloud top height, and high frequency (25-Hz) in-situ measurements of vertical velocity are used to generate the statistics. The major limitations of aircraft in-situ measurements are the aircraft maybe not able to sample the strongest convective cores due to safety concern, and it only provides the information of vertical air motion at single levels. These weaknesses need to be kept in mind in the following analyses. Section 2 describes the datasets and wind measuring systems. Section 3 presents the analysis method. Section 4 shows the results. Section 5 discusses the possible factors those interact with vertical air motions, and conclusions are given in Section 6.

2. Dataset and instruments

2.1 Dataset

The data used in the present study were collected from three field campaigns: HiCu, COPE and ICE-T. Vigorous convective clouds were penetrated during the three field campaigns, including mid-latitude continental, mid-latitude coastal, and tropical maritime convective clouds. These cloud penetrations provide good quality measurements for studying the microphysics and dynamics in the convective clouds, as well as the interactions between the clouds and the ambient air. The locations of the three field campaigns are shown in Fig. 1. Information regarding the penetrations used in this study is summarized in Table 1.

The HiCu project was conducted mainly in Arizona and Wyoming (Fig. 1) from the 18th of July to the 5th of August, 2002, and from the 7th of July to the 31st of August, 2003 to investigate the microphysics and dynamics in convective clouds over the mid-latitude High Plains. The University of Wyoming King Air (UWKA) was the aircraft platform used in this project. In 2002 and 2003, 10 and 30 research flights were conducted, respectively. In this study, the 2002 HiCu and 2003 HiCu are analyzed together because they were both conducted over the High Plains and the sample size of 2002 HiCu is relatively small. Fast-response in-situ instruments and the Wyoming Cloud Radar (WCR, Wang et al., 2012) were operated during the field campaign to measure the ambient environment, cloud dynamics and microphysics and the two-dimensional (2D) cloud structure. As shown in Table 1, penetrations in HiCu occurred between 2 km and 10 km MSL. The sample size is relatively large for penetrations below 8 km and relatively small above 8 km. Accumulated aircraft flight length in cloud was about 2000 km. In-situ measurements and WCR worked well in these flights; however, the upward-pointing radar was operated in less than half of the research flights, and thus only a sub-set of the cloud top heights can be estimated from the observations. Fig. 2a(1–3) shows an example of the clouds sampled in HiCu, including WCR reflectivity, Doppler velocity and 25-Hz in-situ measurement of the vertical velocity. In HiCu, both developing and mature convective clouds were penetrated; some penetrations were near cloud top, while most were more than 1 km below cloud top. The typical WCR reflectivity ranges from 0 to 15 dBZ in the convective cores. In these clouds, reflectivity is strongly impacted by Mie scattering at the WCR wavelength. From the Doppler velocity and the in-situ vertical velocity, we see that, in both the developing and mature cloud, relatively strong updrafts and downdrafts were observed, and multiple updrafts and downdrafts existed in the same cloud. These drafts maybe strong for isolated convection, but not necessarily strong

compared to the strongest updrafts in mesoscale convective systems (MCSs). No balloon soundings are available to measure the ambient environment in HiCu, so we use aircraft measurements to characterize the thermodynamic environment and estimate the convective available potential energy (CAPE). In some cases, the full CAPE cannot be calculated since the aircraft only flew at low levels (below 10 km MSL). The aircraft measurements suggest that the CAPE in HiCu ranged from less than 100 J kg^{-1} to more than 500 J kg^{-1}.

The COPE project was conducted from the 3rd of July to the 21st of August, 2013 in Southwest England (Fig. 1). The UWKA was used to study the microphysics and entrainment in mid-latitude coastal convective clouds (Leon et al., 2015). Seventeen research flights were conducted. The penetrations focused on regions near cloud top, which is verified based on the radar reflectivity from the onboard WCR. Since COPE was conducted in a coastal area, the convection initiation mechanism is different from that over a purely continental or ocean area. In addition, although the ambient air mainly came from the ocean, continental aerosols might be brought into the clouds since many of the convective clouds formed within the boundary layer, further impacting the microphysics and dynamics of these clouds. Measurements from COPE include temperature, vertical velocity, liquid water content, and particle concentration and size distributions. The WCR provided measurements of reflectivity and Doppler velocity. The downward Wyoming Cloud Lidar (WCL) was operated to investigate the liquid (or ice) dominated clouds. The typical WCR reflectivity ranged from 5 to 20 dBZ in the convective cores. Between 0 km and 6 km, there were about 800 penetrations. Accumulated flight distance in cloud totaled about 1000 km. The sample sizes are relatively large between 2 km and 6 km, but relatively small between 0 km and 2 km. Examples of the penetrations are given in Fig. 2b(1–3). COPE has fewer penetrations than HiCu, and most of the penetrations are near the cloud top. Fig.

2b(2) reveals relatively simple structures of the updrafts and downdrafts in COPE compared to HiCu, but as shown by the 25-Hz in-situ vertical velocity measurement in Fig. 2b(3), there are still many complicated fine structures in the vertical velocity distribution. The typical CAPE estimated from soundings in COPE was a few hundred J kg^{-1}.

The ICE-T project was conducted from the 1st of July to the 30th of July, 2011 near St. Croix, U.S. Virgin Islands (Fig. 1), with state-of-the-art airborne in situ and remote sensing instrumentations, with the aim of studying the role of ice generation in tropical maritime convective clouds. The NSF/NCAR C-130 aircraft was used during ICE-T to penetrate convective clouds over the Caribbean Sea. Thirteen C-130 research flights were conducted during the field campaign. In-situ measurements from ICE-T include the liquid and total condensed water contents, temperatures, vertical velocities, and cloud and precipitating particle concentrations and size distributions. The WCR was operated on seven research flights to measure the 2D reflectivity and Doppler velocity fields. Typical WCR reflectivity within convective cores ranged from 10 to 20 dBZ. Accumulated flight distance through clouds was greater than 1500 km, through the more than 650 penetrations between 0 km and 8 km. The sample sizes are good except between 2 km and 4 km (Table 1). Examples of the penetrations are shown in Fig. 2c(1–3). During ICE-T, clouds in different stages were penetrated, including developing, mature and dissipating, some near cloud top and some considerably below cloud top. Maximum observed updrafts were 25 m s^{-1}. Downdrafts in ICE-T were typically weaker than those in HiCu and COPE. The vertical velocity structures are complicated, as confirmed by both the Doppler velocity and the 25-Hz in-situ measurement. Weak updrafts and downdrafts were also observed in the dissipating clouds. The typical CAPE in ICE-T was greater than 2000 J kg^{-1}, which is larger than that in HiCu and COPE.

During the sampling of isolated convective clouds in all the three field campaigns, the aircraft was typically aligned to penetrate through the center of the convective turret, however, this does not guarantee that the aircraft always penetrated through the strongest updraft at that level. In addition, aircraft in-situ measurements only provide the information of vertical air motion at single levels. Moreover, the clouds sampled are isolated convective clouds, MCSs were not sampled. These limitations need to be kept in mind in interpreting the results from the following analyses.

2.2 Wind measuring system

On both the C-130 and UWKA, a five-hole gust probe is installed for measurements of 3D wind**.** On the C-130, this probe is part of the fuselage radome, on the UWKA the probe is mounted on the end of an extended boom protruding from the front of the aircraft. In both cases the probe contains five pressure ports installed in a "cross" pattern. Relative wind components (e.g. true air speed and flow angles) are sensed by a combination of differential pressure sensors attached to the five holes (Wendisch and Brenguier, 2013). Detailed calculation of relative wind components is described in Wendisch and Brenguier (2013). The time response and the accuracy of the pressure sensors is about 25 Hz and 0.1 mb. The 3D wind vectors are determined by subtracting the aircraft velocity from the relative wind measurement after rotating the vectors to a common coordinate system. On the C-130 and UWKA, aircraft velocity is measured by a Honeywell LASEREF SM Inertial Reference System (IRS), with an accuracy of 0.15 m s^{-1} for vertical motion. Global Positioning System (GPS) was applied to remove the drift errors in the IRS position in all the three field campaigns (Khelif et al., 1998). The final vertical wind velocity

product has an accuracy of about ±0.2 m s^{-1}, and a time response of 25 Hz. This uncertainty (±0.2 m s^{-1}) is a mean bias. For each output, the uncertainty is related to the true air speed, aircraft pitch angle, roll angle and ambient conditions. Therefore, the random error varies and could be larger than the mean bias. More information about the wind measurement on C-130 and UWKA can be found on the C-130 Investigator Handbook (available on https://www.eol.ucar.edu/content/c-130-investigator-handbook) and UWKA Investigator Handbook (available on http://www.atmos.uwyo.edu/uwka/users/KA_InstList.pdf)

3. Analysis method

3.1 Identifying cloud using in-situ measurements

The Particle Measuring Systems (PMS) Two-Dimensional Cloud (2D-C) Probe and the Forward Scattering Spectrometer Probe (FSSP) are often used to characterize cloud microphysics (e.g. Anderson et al., 2005), although different thresholds of 2D-C and FSSP concentrations are usually used to identify the edge of a cloud. In this paper, we also use FSSP and 2D-C probes to find the cloud edges. In order to find a reasonable threshold for identifying cloudy air, we first use the WCR reflectivity to identify the clouds and the cloud-free atmosphere; for those regions we then plot the particle concentrations measured by FSSP and 2D-C in order to determine reasonable thresholds, and we apply the thresholds of particle concentrations to all the research flights without WCR.

To identify clouds using WCR, the six effective range gates nearest to the flight level (three above and three below) are chosen in each beam. Any beam in which the minimum reflectivity at the six gates exceeds -30 dBZ[1] is identified as in-cloud.

Fig. 3 shows the occurrence distribution as a function of the particle concentrations measured by FSSP versus the concentrations of the particles ≥ 50 μm in diameter measured by 2D-C in the clouds identified by WCR reflectivity. From the figure, we see that the FSSP concentration ranges from 0.01 cm^{-3} to 1000 cm^{-3}, and the 2D-C concentration ranges from 0.1 L^{-1} to 10000 L^{-1}. Generally, shallow clouds have relatively higher concentrations of small particles and lower concentration of particles larger than 50 μm. In deeper convective clouds, high concentrations can be seen for both small and large particles. The FSSP concentrations in cloud-free air are found to be 2 cm^{-3} at most, and the FSSP concentrations measured below the lifting condensation level (LCL), where precipitation particles dominated, are lower than 2 cm^{-3} as well. Therefore, 2 cm^{-3} is selected as the concentration threshold to identify clouds based on the FSSP measurements, indicated by the dashed line in Fig. 3. However, in some clouds (e.g. pure ice clouds), the FSSP concentration could be lower than 2 cm^{-3}, and 2D-C concentrations are needed to identify these cold clouds. We chose a concentration of 1 L^{-1} 2D-C particles with diameters larger than 50 μm as the second threshold to identify cloud, indicated by the dotted line in Fig. 3. In order to avoid precipitating regions (below the LCL calculated from soundings), the second threshold is only applied to penetrations at temperatures colder than 0 ºC, thus the cloud is defined when FSSP concentration ≥ 2 cm^{-3} or 2D-C concentration ≥ 1 L^{-1}. At temperatures

[1] Based on the reflectivity measured in cloud-free air, the noise level of WCR reflectivity is -32 dBZ at a range of 500 m and -28 dBZ at a range of 1000 m. In this study, we choose -30 dBZ as the threshold to identify cloud. This threshold (-30 dBZ) is examined for all three field campaigns.

263 warmer than 0 ºC, the FSSP concentrations in most convective clouds are higher than 2 cm^{-3}, so
264 only the first threshold is used.

265 Once a cloud is identified, the penetration details can be calculated, including the flight length,
266 the flight height, the cloud top height if WCR data were available, and the penetration diameter.
267 The penetration diameter is calculated as the distance between the entrance and exit of a
268 penetration. In order to reject penetrations with significant turns, we require that the diameter of
269 a penetration be at least 90% of the flight length, so the cloud scale will not be significantly
270 overestimated. Since the aircraft might not penetrate exactly through the center of a cloud, the
271 actual cloud diameter may be larger than the penetration diameter. Based on WCR reflectivity
272 images, there are no isolated convective clouds sampled larger than 20 km in diameter. There are
273 a few penetrations longer than 20 km, but these clouds are more like part of MCSs, and so they
274 are excluded from this study.

275

276 **3.2 Defining updraft and downdraft**

277 In previous studies of the vertical velocity based on in-situ measurements, the updraft and
278 downdraft were often defined as an ascending or subsiding air parcel with the vertical velocity
279 continuously ≥ 0 m s^{-1} in magnitude and ≥ 500 m in diameter (e.g. LeMone and Zipser, 1980;
280 Jorgensen and LeMone, 1989; Lucas et al., 1994; Igau et al., 1999). In this study, we use a
281 vertical velocity threshold of 0.2 m s^{-1}, that is, the draft has a vertical velocity continuously ≥ 0.2
282 m s^{-1} in magnitude, because ± 0.2 m s^{-1} is the accuracy of the instrument. Any very narrow and
283 weak portion (diameter < 10 m and maximum vertical velocity < 0.2 m s^{-1} in magnitude)

between two relatively strong portions is ignored, and the two strong portions are considered as one draft.

The diameter threshold (500 m) is not used in this paper, because drafts narrower than 500 m frequently occur and they may make important contributions to the total air mass flux in the atmosphere and therefore they are necessary to be considered in model simulations. Fig. 4 shows the PDFs of the diameters of all the updrafts and downdrafts sampled in HiCu, COPE and ICE-T. In all the panels, the diameters are exponentially distributed, the PDFs can be fitted using

$$f = \alpha \cdot |x|^{\beta} \cdot \exp(\gamma|x|) \qquad (1)$$

where f is the frequency and x is the diameter. The coefficients α, β and γ for each PDF is shown in each panel. This function will also be used to fit the PDFs of vertical velocity and air mass flux in the following analyses. Generally, as seen in Fig. 4, the PDFs broaden with increasing height for the three field campaigns, consistent with previous findings (LeMone and Zipser, 1980). The diameters of the observed updrafts are smaller in COPE compared to those sampled in HiCu and ICE-T, possibly because most of the penetrations are near cloud top. As shown in Fig. 4, many narrow drafts are observed. More than 85%, 90% and 74% of the observed updrafts are narrower than 500 m (dotted lines) in HiCu, COPE and ICE-T, respectively, and more than 90% of the observed downdrafts in all three field campaigns are narrower than 500 m. A threshold of 500 m in diameter would exclude many small-scale drafts, therefore, in this study all the drafts broader than 50 m (dashed lines) are included. Drafts narrower than 50 m are excluded because most of them are turbulence.

Fig. 5a shows the occurrence distributions as a function of the mean vertical velocity versus the diameter of the drafts with the vertical velocity continuously ≥ 0.2 m s^{-1} in magnitude. From the

figure, it is noted that many drafts narrower than 500 m have quite strong vertical velocities. The maximum mean vertical velocity of these narrow drafts can reach 8 m s^{-1}, and the minimum mean vertical velocity in the downdrafts is –6 m s^{-1}. With such strong mean vertical velocity, narrow drafts could contribute noticeably to the total air mass flux. Fig. 5b presents the occurrence distributions as a function of the air mass flux versus the diameter of the drafts. The air mass flux is calculated as $\bar{\rho}\overline{w}D$ (LeMone and Zipser, 1980), where $\bar{\rho}$ is the mean air density at the measurement temperature, $\overline{w}$ is the mean vertical velocity and *D* is the diameter of each draft. Due to the limitation of aircraft in-situ measurements, the air mass flux is calculated using the data from single-line penetrations. This may introduce additional uncertainties in air mass flux estimations for these clouds. Fig. 5b shows that the air mass flux in many drafts narrower than 500 m is actually larger than air mass flux in some of the broader drafts. The maximum value for these narrow updrafts reaches 4000 kg m^{-1} s^{-1}, and the minimum value for the downdrafts reaches –3000 kg m^{-1} s^{-1}. The normalized accumulated flux (red curves) reveals that the drafts narrower than 500 m (dotted horizontal lines) contribute significantly to the total air mass flux. Calculations indicate that the updrafts narrower than 500 m contribute 20%–35% of the total upward flux, and that the downdrafts narrower than 500 m contribute 50%–65% of the total downward air mass flux. Drafts narrower than 50 m (dashed horizontal lines), which are excluded in this paper, contributes less than 5% of the total air mass flux.

In this study, we delineate three different groups of updrafts and downdrafts using three thresholds of air mass flux: 10 kg m^{-1} s^{-1}, 100 kg m^{-1} s^{-1} and 500 kg m^{-1} s^{-1} in magnitude. The air mass flux is used here to delineate the draft intensity because (1) air mass flux contains the information of both vertical velocity and draft size; (2) air mass flux can reveal the vertical mass transport through convection; and (3) air mass flux is an important component in cumulus and

convection parameterizations (e.g. Tiedtke, 1989; Bechtold et al., 2001). The first designated group, the "weak draft," with air mass flux 10–100 kg m^{-1} s^{-1} in magnitude, contributes 10% of the total upward air mass flux and 10% of the total downward air mass flux. The "moderate draft," with air mass flux 100–500 kg m^{-1} s^{-1} in magnitude, contributes 25% of the total upward air mass flux and 40% of the total downward air mass flux. The "strong draft," where the air mass flux $\geq$ 500 kg m^{-1} s^{-1} in magnitude contributes 60% of the total upward air mass flux and 20% of the total downward air mass flux. The definitions of "weak", "moderate" and "strong" only apply for the isolated convective clouds analyzed in this study, and are not necessarily appropriate for organized convection (e.g. MCS). Drafts weaker than 10 kg m^{-1} s^{-1} are not analyzed because they are too weak and most of them are very narrow (Fig. 5b). The numbers of weak, moderate and strong updrafts and downdrafts sampled at 0–2 km, 2–4 km, 4–6 km, 6–8 km and 8–10 km MSL are shown in Table 2. Generally, weak and moderate drafts are more often observed than strong drafts. At most of the height ranges, more updrafts are observed than downdrafts.

Some researchers have defined a "draft core" by selecting the strongest portion within a draft. For example, LeMone and Zipser (1980) define an updraft core as an ascending air motion with vertical velocity continuously $\geq$ 1 m s^{-1} and diameter $\geq$ 500 m. This definition of a "draft core" is followed in a few more recent studies (e.g. Jorgensen and LeMone, 1989; Lucas et al., 1994; Igau et al., 1999). We too analyzed the vertical air motion characteristics in the stronger portion of the drafts considered here. However, we found that in many updrafts the strong portion where the vertical velocity is continuously $\geq$ 1 m s^{-1} dominates and contributes 80% of the total air mass flux, so the statistics of the vertical air motion characteristics in the stronger portion are

very similar to those in the draft as a whole. Therefore, the present study focuses on "drafts" in which both weak and strong portions are included.

4. Results

4.1 Significance of drafts in different strengths

From the analysis above, we note that relatively small and weak updrafts are frequently observed in convective clouds. In this section, we provide further evidence to show the importance of the relatively weak updrafts in terms of air mass flux.

Fig. 6a shows the average number of updrafts as a function of air mass flux observed in the three field campaigns. The solid, dashed and dotted lines represent the penetrations with different diameters. As shown in Fig. 6a, weak and moderate updrafts are more often observed than strong updrafts, and more updrafts are observed in longer penetrations. Since this is an average result, the number of updrafts could be smaller than 1 (e.g. many short penetrations do not have strong updrafts). Fig. 6b is similar to Fig. 6a but shows the occurrence frequency of updrafts with different air mass fluxes (i.e. the vertical axis in Fig. 6a is normalized). For the penetrations less than 1 km in length, many of the clouds only have weak or moderate updrafts, and relatively strong updrafts are rarely observed. For penetrations of 1–10 km, the frequency of strong updrafts increases and the frequency of weak and moderate updrafts decreases. For even longer penetrations (>10 km), however, the frequency of weak updrafts increases again, indicating the increasing importance of weak updrafts.

Fig. 7 shows the average percentile contributions to the total upward air mass flux by the three different groups of updrafts as a function of penetration diameter. In Fig. 7a, all the penetrations are included. Since many narrow clouds have no strong updrafts in terms of air mass flux, the total air mass flux in these narrow clouds is mostly contributed by weak (red bar) and moderate (green bar) drafts. These narrow clouds may have a large vertical velocity but small air mass flux. As the diameter increases to 4 km, the contributions to total air mass flux from relatively weak updrafts (red bar) decrease, while those from stronger updrafts (blue bar) increase. For a penetration of 4 km length, 80%–90% of the total upward mass flux is contributed by the strong updrafts with air mass flux $\geq$ 500 kg m^{-1} s^{-1}. However, for the penetrations with diameter larger than 4 km, the contribution from relatively weak updrafts increases, probably because more weak updrafts exist in wider clouds (Fig. 6). This is more obvious in Fig. 7b, in which only the penetrations with at least one strong updraft are included. As the diameter increases from 400 m to 20 km, the contribution from the weak and moderate updrafts (red bars and green bars) increases from 2% to 20%. This suggests that as the cloud evolves and becomes broader (e.g. mature or dissipating stage), the weak and moderate updrafts are also important and therefore necessary to be considered in model simulations.

4.2 PDFs of vertical velocity and air mass flux

Fig. 8 shows the PDFs of the vertical velocity in the drafts sampled at 0–2 km, 2–4 km, 4–6 km and higher than 6 km in the three field campaigns. Columns (a), (b) and (c) represent the drafts with air mass flux $\geq$ 10 kg m^{-1} s^{-1}, $\geq$ 100 kg m^{-1} s^{-1} and $\geq$ 500 kg m^{-1} s^{-1} in magnitude, respectively; in other words, column (a) includes all the weak, moderate and strong of drafts,

393 column (b) includes moderate and strong updrafts, and column (c) includes strong updrafts only.
394 For statistical analysis, it is better to analyze different drafts together rather than separately.
395 Since the aircraft might under-sample the strongest updraft cores, the tails of the PDFs could be
396 biased low, but these PDFs still provide valuable information. In all the panels, the observed
397 vertical velocities are exponentially distributed for both updrafts and downdrafts; the PDFs can
398 be fitted using Eq. (1). From Fig. 8 we see that at 0–2 km, the PDFs for both COPE and ICE-T
399 are narrow. At 2–4 km, stronger updrafts and broader PDFs are observed in both COPE and ICE-
400 T compared to those at 0–2 km, and the maximum vertical velocity is about 15 m s^{-1}. In COPE,
401 the observed downdrafts are stronger than those in ICE-T, with the minimum vertical velocity as
402 low as –10 m s^{-1}. For HiCu, the PDFs of the vertical velocity at 2–4 km are narrow, because the
403 HiCu project was conducted in the High Plains and the cloud bases were relatively high. At 4–6
404 km, the observed updrafts become stronger and the PDFs become broader in all the three field
405 campaigns compared to those at lower levels, especially for COPE and ICE-T. Above 6 km, the
406 PDFs for the updraft become broader in HiCu while they slightly narrow in ICE-T compared to
407 those at 4–6 km. For the observed downdrafts, the PDFs broaden with height for all the three
408 field campaigns. Generally, the PDFs of the vertical velocity are similar for the three columns.
409 The main difference is found in the first bins of the vertical velocity (0–2 m s^{-1} and – 2–0 m s^{-1}):
410 highest for column (a), which includes all the drafts with air mass flux $\geq$ 10 kg m^{-1} s^{-1} in
411 magnitude, lowest for column (c), which only includes the strong drafts with air mass flux $\geq$ 500
412 kg m^{-1} s^{-1} in magnitude.

413 In Fig. 8, the observed updrafts are stronger in ICE-T and COPE (maritime or coastal convective
414 clouds) than in HiCu (pure continental convective clouds). But the aircraft might under sample
415 the strongest part of the convective cores. In addition, the PDFs are plotted as a function of MSL

height, the relatively narrow PDFs in HiCu compared to COPE and ICE-T at the same height are possibly because of the higher cloud bases in HiCu. Other than the sampling issues, the triggering mechanism for convection is also important for the updraft strength. The clouds sampled in the three field campaigns are all isolated convective clouds, the CAPE in HiCu was smaller than in COPE and ICE-T. Compared to the GATE project, in which the clouds were also sampled over a tropical ocean, the PDFs of the vertical velocity in ICE-T have a similar vertical dependence, broadening with height. But the PDFs are broader in ICE-T than those in GATE, and the maximum vertical velocity (25 m s^{-1}) in ICE-T is greater than that observed in GATE (15 m s^{-1}). In GATE, the in-situ measurements also have sampling issues. More measurements are needed to further evaluate the difference between maritime and continental convective clouds.

Fig. 9 shows the PDFs of the air mass flux for all the drafts sampled at 0–2 km, 2–4 km, 4–6 km and higher than 6 km. The PDFs are exponentially distributed for the three field campaigns at different heights, which can be fitted using Eq. (1). The coefficients for the fitted function are shown in each panel. In the three field campaigns, the PDFs of air mass flux have no obvious trend with height, although the PDFs of diameter and vertical velocity broaden with height. The differences among the three field campaigns are small for weak and moderate drafts, and become slightly larger for relatively strong updrafts, which could be due to the sampling issues.

4.3 Profiles of vertical velocity and air mass flux

Fig. 10 is a Whisker-Box plot showing the profiles of the vertical velocity (a-c) and air mass flux (d-f) in the drafts based on the three defined thresholds of air mass flux. The solid box includes all three different groups of drafts, the dashed boxes excludes the weak drafts, and the dotted

boxes includes strong drafts. The minimum, 10%, 50%, 90% and maximum values are shown in each box. In each panel, the absolute values of the vertical velocities and air mass flux (except the minimum and maximum ones) are relatively small for the solid boxes.

In Fig. 10a-c, the three definitions of drafts show different intensities in the vertical velocities. Typically, the 10%, 50% and 90% values in the dotted boxes are 1–2 times larger in magnitude than those in the solid boxes. However, the profiles of the three definitions of drafts vary similarly with height for each field campaign. In the updrafts sampled during HiCu (Fig. 10a), the maximum vertical velocity increases with height up to 8 km, then decreases with height above that. The 90% vertical velocity in the solid boxes increases from 4 m s^{-1} to 8 m s^{-1} between 0–10 km. The 10% and 50% vertical velocities in the solid boxes remain similar between 2–8 km then slightly increase at 8–10 km. In the downdrafts, the minimum vertical velocity decreases from –7 m s^{-1} to –12 m s^{-1} up to 8 km and increases to –9 m s^{-1} at 8–10 km. The 10%, 50 % and 90% values all slightly decrease with height. In the updrafts sampled during COPE (Fig. 10b), the maximum, 10%, 50% and 90% vertical velocities increase with height and the observed maximum value is 23 m s^{-1}. The minimum vertical velocity in the downdrafts intensifies from –5 to –10 m s^{-1} with height up to 4 km, then remains similar at 4–6 km. In the updrafts sampled during ICE-T (Fig. 10c), the maximum vertical velocities increase with height from 5.5 m s^{-1} to 25 m s^{-1} up to 6 km, then slightly decreases at 6–8 km. The 90% value increases from 2 to 6 m s^{-1} between 0–4 km, then remains similar at higher levels. The 10% and 50% values do not show an obvious trend with height. In the downdrafts the minimum vertical velocity remains similar below 4 km, and decreases to –18 m s^{-1} between 4 km and 8 km. The 10%, 50% and 90% values tend to decrease or remain similar at lower levels and then increase with height higher up. The

460 peak (~25 m s^{-1}) and the minimum (~-18 m s^{-1}) vertical velocities are observed at 4–6 km and 6–
461 8 km, respectively.

462 To summarize, the observed vertical velocity in the drafts varies differently with height in the
463 three field campaigns. Stronger downdrafts are often observed in HiCu and COPE compared to
464 those in ICE-T. The weak, moderate and strong drafts have similar variations with height, but the
465 magnitudes are the smallest when including all the drafts and become larger if the weak drafts
466 are excluded. The 10%, 50% and 90% vertical velocities in updrafts and downdrafts over the
467 tropical ocean (ICE-T) observed in this study generally have similar magnitudes to those shown
468 in previous studies (e.g. LeMone and Zipser, 1980; Lucus and Zipser, 1994). But strong updrafts
469 (downdrafts) in excess of 20 m s^{-1} (–10 m s^{-1}) are also observed in this study, which were rarely
470 reported in previous aircraft observations. This finding is consistent with recent remote sensing
471 observations (e.g. Heymsfield et al., 2010). The updrafts and downdrafts in convective clouds
472 over land shown in this study (HiCu) are weaker than those shown by Byers and Braham (1949)
473 and Heymsfield et al. (2010), possibly because the clouds sampled in HiCu were isolated
474 convective clouds over High Plains, which apparently differ from deeper convective clouds at
475 lower elevations.

476 Fig. 10d-f shows the profiles the air mass flux statistics for the drafts sampled during the three
477 field campaigns. As expected, the absolute values of the air mass flux are relatively small if all
478 the drafts are included (dotted boxes), and become larger if the drafts with relatively small air
479 mass flux are excluded. However, the variations of the observed air mass flux with height are
480 similar for the three different definitions in each panel. As determined by the three thresholds,
481 the minimum absolute values in the solid boxes are about 10 times smaller than those in the
482 dashed boxes and about 50 times smaller than those in the dotted boxed. For the 10%, 50%, 90%

and the maximum absolute values, the differences among the three types of boxes become smaller. The observed air mass flux varies with height differently for the three field campaigns and does not have an obvious trend with height. For updraft, the observed maximum air mass flux is on the order of 10^4 kg m^{-1} s^{-1}, and the median values for the three different types of boxes are typically ~100 kg m^{-1} s^{-1}, ~200 kg m^{-1} s^{-1} and ~1000 kg m^{-1} s^{-1}, respectively. The observed air mass flux in the downdrafts is a few times smaller in magnitude than those in the updrafts, but extreme downdrafts on the order of 10^4 kg m^{-1} s^{-1} could be observed in some specific cases. Compared to previous studies, the air mass flux in this study shows similar magnitudes, but the vertical dependences are different. Lucas and Zipser (1994) show that the convection off tropical Australia intensified with height from 0 to 3 km, then weakened with height in terms of air mass flux. Anderson et al. (2005) show that updrafts and downdrafts over the tropical Pacific Ocean intensified with height up to 4 km, then weakened at higher levels. In contrast, this study shows the strongest updrafts and downdrafts in terms of air mass flux were observed at higher levels.

4.4 Composite structure of vertical velocity

Fig. 11 shows the composite structure for the updrafts and downdrafts with air mass flux $\geq$ 10 kg m^{-1} s^{-1} as a function of normalized scale. The 0 and 1 coordinates on the x-axis indicate the upwind and downwind sides of the draft, respectively, such that the draft is centered at 0.5. Since we do not have continuous penetrations in a single cloud, we have to statistically analyze the evolution of the draft structure. In Fig. 11, we can see the normalized shape does not change significantly with height, but the observed peak vertical velocity does increase with height for all the three field campaigns. If the magnitude of the vertical velocity is normalized, the structures

of the updraft and downdraft at different heights would be very similar. Connecting this figure to the PDFs of diameter (Fig. 4) and air mass flux (Fig. 9), the results show statistically that the drafts were expanding (Fig. 4) and the magnitude of vertical velocity was increasing (Fig. 11), but the air mass flux has no obvious dependence with height (Fig. 9). This reveals the complexity of the evolution of the drafts. Based on our datasets, there could be different possibilities of updraft changes with height: 1) an updraft expanded and the vertical velocity weakened with height, 2) an updraft expanded and the vertical velocity strengthened with height, 3) an updraft divided into multiple updrafts and downdrafts, 4) two updrafts merged and became one updraft. In addition, entrainment/detrainment and water loading also have important impacts on how drafts change with height within convective clouds.

In this composite analysis based on in-situ measurements, the penetration direction has no obvious impact on the vertical velocity structure, whether the aircraft penetrates along or across the horizontal wind (not shown). For convective clouds, wind shear has a large impact on the cloud evolution (Weisman and Klemp 1982); however, the aircraft data are insufficient to reveal the wind shear impact, because each penetration was made at a single level and the aircraft did not always penetrate through the center of the draft. Remote sensing data can be helpful to study the 2D or 3D structures of the vertical velocity in convective clouds. For example, airborne radar with slant and zenith/nadir viewing beams can provide 2D wind structure in convective clouds (e.g. Wang and Geerts, 2013). Volumetric radar (e.g. Collis et al. 2013, Jorgensen et al. 2000) can provide 3D structure of air (or hydrometeor) motion. Thus, in-situ measurements as well as remote sensing measurements are needed to further analyze the wind shear impact.

4.5 Vertical air motion characteristics as clouds evolve

Fig. 12 shows the profiles of vertical velocity (a-c) and air mass flux (d-f) for the updraft and downdraft in the convective clouds with different cloud top heights (CTH). Here, all weak, moderate and strong updrafts are included. Different colors represent clouds with different CTHs. These profiles generally reveal the change of vertical velocity and air mass flux as the clouds evolve. The key point presented in Fig. 12a-c is that the peak vertical velocity is observed at higher levels as the clouds evolve. For clouds with CTHs lower than 4 km (red boxes), the maximum vertical velocity is observed at 2–4 km. When the cloud become deeper, the observed vertical velocity and air mass flux are stronger at higher levels. The maximum vertical velocity is observed within 2 km of cloud top; consistent with Doppler velocity images measured by WCR (e.g. Fig. 2b) that show the strongest updraft is typically observed 1–1.5 km below cloud top. The strongest downdrafts are sometimes observed more than 2 km below cloud top. The 10% and 50% values do not have obvious trends as the clouds evolve, possibly because of the increasing contribution from moderate and weak drafts as the clouds become deeper and broader (Fig. 6 and 7). The observed air mass flux (Fig. 12d-f) has no obvious trend as the clouds evolve, again suggesting multiple factors (e.g. entrainment/detrainment, microphysics) may impact the evolution of these drafts. Since the aircraft provides data from just single-line penetrations, and not 2D vertical information, additional measurements, including remote sensing measurements are needed to better understand the evolution of the vertical velocity in convective clouds.

5. Discussion

548 In this study, we provide the statistics of vertical air motion in isolated convective clouds using
549 in-situ measurements from three field campaigns. The statistical results suggest vertical air
550 motions in convective clouds are very complicated and could be affected by many factors.

551 Microphysics strongly interacts with vertical velocity through different processes, for example,
552 droplet condensation/evaporation, ice nucleation/sublimation, water loading, etc. Yang et al.
553 (2016) show the LWC and IWC are both higher in stronger updrafts in developing convective
554 clouds, while the liquid fraction has no obvious correlation with vertical velocity. In mature
555 convective clouds the LWC is also higher in stronger updrafts, but the IWC is similar in
556 relatively weak and strong updrafts. The liquid fraction is correlated to the vertical velocity
557 between -3 °C and -8 °C, possibly because Hallet-Mossop process is more significant in weaker
558 updrafts (Heymsfield and Willis, 2014). Lawson et al. (2015) shows the existence of millimeter
559 drops in the convective clouds can result in fast ice initiation, and the significant latent heat
560 released during the ice initiation process can strengthen the updrafts. In ICE-T and COPE, we
561 also observe many millimeter drops, which may strongly interact with vertical velocity through
562 fast ice initiation process. However, in some cases, the existence of millimeter drops can result in
563 a significant warm rain process (Yang et al. 2016; Leon et al. 2016), which may weaken the
564 updrafts and result in rapid cloud dissipation.

565 Entrainment/detrainment also has a strong interaction with vertical velocity. In the analysis
566 above, the downdrafts observed in HiCu and COPE are stronger than those observed in ICE-T.
567 This may be partly because the ambient relative humidity is low in HiCu and COPE compared to
568 ICE-T, resulting in a strong evaporation-cooling effect when the ambient air mixes with cloud
569 parcels through lateral entrainment/detrainment (Heymsfield et al., 1978). Entrainment has
570 impacts on updrafts as well. Recent studies using in-situ measurements and model simulations

suggest stronger entrainment may result in weaker updrafts (e.g. Lu et al., 2016). In this study, we also find weaker updrafts are associated with stronger entrainment/detrainment using in-situ measurements of relative humidity, equivalent potential temperature, droplet concentration and LWC (not shown). Previous studies (e.g. Heymsfield et al., 1978; Wang et al., 2013) suggest updraft cores unaffected by entrainment may exist in some convective clouds.

Again it is important to be aware of the limitations of using aircraft in-situ measurements for this kind of study. More observations (in situ and remote sensing) as well as model simulations are needed to better characterize the vertical air motion in convective clouds and its interactions with microphysics and entrainment/detrainment mixing.

6. Conclusions

The vertical velocity and air mass flux in isolated convective clouds are statistically analyzed in this study using aircraft data collected from three field campaigns, HiCu, COPE and ICE-T, conducted over mid-latitude High Plains, mid-latitude coastal area and tropical ocean. Three thresholds of air mass flux are selected to delineate weak, moderate and strong draft: 10 kg m^{-1} s^{-1}, 100 kg m^{-1} s^{-1} and 500 kg m^{-1} s^{-1} in magnitude. These definitions only apply for the isolated convective clouds analyzed in this study and are not necessarily appropriate for other convections (e.g. MCSs). The main findings are as follows.

1) Small-scale updrafts and downdrafts in convective clouds are often observed in the three field campaigns. More than 85%, 90% and 74% of the updrafts are narrower than 500 m in HiCu, COPE and ICE-T, respectively, and more than 90% of the downdrafts are narrower than 500 m

592 in the three field campaigns combined. These small scale drafts make significant contributions to
593 the total air mass flux. Updrafts narrower than 500 m contribute 20%–35% of the total upward
594 flux, and downdrafts narrower than 500 m contribute 50%–65% of the total downward air mass
595 flux.

596 2) In terms of the air mass flux, the weak and moderate drafts make an important
597 contribution to the total air mas flux exchange. Generally, the number of drafts increases with
598 cloud diameter. For many narrow clouds, the weak and moderate drafts dominate and contribute
599 most of the total air mass flux. For broader clouds, the stronger updrafts contribute most of the
600 total air mass flux, but the contribution from weak and moderate drafts increases as the cloud
601 evolves.

602 3) PDFs and profiles of the vertical velocity are provided for the observed drafts. In all the
603 height ranges, the PDFs are roughly exponentially distributed and broaden with height. The
604 observed downdrafts are stronger in HiCu and COPE compared to ICE-T. Relatively strong
605 updrafts (> 20 m s^{-1}) were sampled during ICE-T and COPE. The observed updrafts in HiCu are
606 weaker than previous studies of deeper continental convections, possibly because the clouds
607 sampled in HiCu were isolated convective clouds over High Plains, which could be different
608 than deeper convective clouds from low elevations.

609 4) PDFs and profiles of the air mass flux are provided for the observed drafts. The PDFs are
610 similarly exponentially distributed at different heights, and have no obvious trend with height. In
611 the updrafts, the observed maximum air mass flux has an order of 10^4 kg m^{-1} s^{-1}. The air mass
612 flux in the downdrafts are typically a few times smaller in magnitude than those in the updrafts.

5) The composite structures of the vertical velocity in the updrafts and downdrafts have similar normalized shapes for the three field campaigns: the vertical velocity is the strongest near the center, and weakens towards the edges. Statistically, the vertical velocity and diameter were increasing with height, but the air mass flux does not has obvious trend with height, suggesting entrainment/detrainment, water loading and other complicated processes have impacts on the evolution of the drafts.

6) The change of vertical air motion characteristics as the cloud evolves are briefly discussed. Generally, the strongest portion of a draft ascends with height as the cloud evolves. The maximum vertical velocity is observed within 2 km below cloud top; the downdrafts are sometimes stronger at levels more than 2 km below cloud top.

The vertical air motion in convective clouds is very complicated, and is affected by many factors, such as convection mechanisms, entrainment/detrainment and microphysics. This study only deals with isolated convective clouds and there are many limitations of aircraft in-situ measurements. More data, including both in-situ and remote sensing measurements, are needed to better understand the vertical air motion in convective clouds.

Acknowledgments

This work is supported by National Science Foundation Award: AGS-1230203 and AGS-1034858, the National Basic Research Program of China under grant no. 2013CB955802 and DOE Grant DE-SC0006974 as part of the ASR program. The authors acknowledge the crew of NCAR C-130 and University of Wyoming King Air for collecting the data and for providing

high-quality products. Many thanks are also extended to Drs. Gerald Heymsfield and Scott Collis for their constructive comments.

References

Anderson, N. F., Grainger, C. A., and Stith, J. L.: Characteristics of Strong Updrafts in Precipitation Systems over the Central Tropical Pacific Ocean and in the Amazon. J. Appl. Meteor., 44, 731–738, 2005.

Arakawa, A.: The cumulus parameterization problem: Past, present, and future. J. Clim., 17, 2493–2525, 2004.

Bechtold, P., Bazile, E., Guichard, F., Mascart, P. and Richard, E.: A mass-flux convection scheme for regional and global models. Quarterly Journal of the Royal Meteorological Society, 127(573), 869-886, 2001.

Byers, H. R. and Braham, R. R.: The Thunderstorm-Report of the Thunderstorm Project. U.S. Weather Bureau, Washington, D.C., Jun 1949. 287 pp. [NTIS PB234515], 1949.

Collis, S., Protat, A., May, P. T., and Williams, C.: Statistics of Storm Updraft Velocities from TWP-ICE Including Verification with Profiling Measurements. J. Appl. Meteor. Climatol., 52, 1909–1922, 2013.

Del Genio, A. D., Wolf, A. B., and Yao, M.-S.: Evaluation of regional cloud feedbacks using single-column models, J. Geophys. Res., 110, D15S13, doi:10.1029/2004JD005011, 2005.

Donner, L. J., Seman, C. J., Hemler, R. S., and Fan, S.: A Cumulus Parameterization Including Mass Fluxes, Convective Vertical Velocities, and Mesoscale Effects: Thermodynamic and Hydrological Aspects in a General Circulation Model. J. Climate, 14, 3444–3463, 2001.

Giangrande, S. E., Collis, S., Straka, J., Protat, A., Williams, C. and Krueger, S.: A summary of convective-core vertical velocity properties using ARM UHF wind profilers in Oklahoma. J. App. Meteor. Climatol., 52, 2278-2295, 2013.

Heymsfield, A. J., Johnson, P. N., and Dye, J. E.: Observations of Moist Adiabatic Ascent in Northeast Colorado Cumulus Congestus Clouds. J. Atmos. Sci., 35, 1689–1703, 1978.

Heymsfield, A. J., and Willis, P.: Cloud conditions favoring secondary ice particle production in tropical maritime convection. J. Atmos. Sci., 71, 4500–4526, 2014.

Heymsfield, G. M., Tian, L., Heymsfield, A. J., Li, L., and Guimond, S.: Characteristics of Deep Tropical and Subtropical Convection from Nadir-Viewing High-Altitude Airborne Doppler Radar. J. Atmos. Sci., 67, 285–308, 2010.

Hildebrand, P. H., Lee, W., Walther, C. A., Frush, C., Randall, M., Loew, E., Neitzel, R., and Parsons, R.: The ELDORA/ASTRAIA Airborne Doppler Weather Radar: High-Resolution Observations from TOGA COARE. *Bull. Amer. Meteor. Soc.*, 77, 213–232, 1996

Hogan, R. J., Grant, A. L., Illingworth, A. J., Pearson, G. N., and O'Connor, E. J.: Vertical velocity variance and skewness in clear and cloud-topped boundary layers as revealed by Doppler lidar, Q. J. Roy. Meteorol. Soc., 135, 635–643, 2009.

Houze Jr., R. A., and Betts, A. K.: Convection in GATE, Rev. Geophys., 19(4), 541–576, 1981.

Igau, R. C., LeMone, M. A., and Wei, D.: Updraft and Downdraft Cores in TOGA COARE: Why So Many Buoyant Downdraft Cores?. J. Atmos. Sci., 56, 2232–2245, 1999.

675 Ivanova, I. T. and Leighton, H. G.: Aerosol–Cloud Interactions in a Mesoscale Model. Part I:
676 Sensitivity to Activation and Collision–Coalescence. J. Atmos. Sci., 65, 289–308, 2008.

677 Jorgensen, D. P., Zipser, E. J., and LeMone, M. A.: Vertical Motions in Intense Hurricanes. J.
678 Atmos. Sci., 42, 839–856, 1985.

679 Jorgensen, D. P. and LeMone, M. A.: Vertically Velocity Characteristics of Oceanic Convection.
680 J. Atmos. Sci., 46, 621–640, 1989.

681 Jorgensen, D. P., and Smull, B. F.: Mesovortex circulations seen by airborne Doppler radar
682 within a bow-echo mesoscale convective system. Bull. Amer. Meteor. Soc., **74,** 2146–2157,
683 1993.

684 Jorgensen, D. P., Shepherd, T. R., and Goldstein, A. S.: A dual-pulse repetition frequency
685 scheme for mitigating velocity ambiguities of the NOAA P-3 airborne Doppler radar. J. Atmos.
686 Oceanic Technol., **17,** 585–594, 2000.

687 Khairoutdinov, M. F., Krueger, S. K., Moeng, C.-H., Bogenschutz, P. A., and Randall, D. A.:
688 Large-Eddy Simulation of Maritime Deep Tropical Convection, J. Adv. Model. Earth Syst., 1, 15,
689 doi:10.3894/JAMES.2009.1.15, 2009.

690 Khelif, D., Burns, S. P., and Friehe, C. A.: Improved Wind Measurements on Research
691 Aircraft. J. Atmos. Oceanic Technol., 16, 860–875, 1999.

692 Kollias, P and Albrecht, B.: Vertical Velocity Statistics in Fair-Weather Cumuli at the ARM
693 TWP Nauru Climate Research Facility. J. Climate, 23, 6590–6604, 2010.

694 Lawson, P. R., Woods, S., and Morrison, H.: The microphysics of ice and precipitation
695 development in tropical cumulus clouds. J. Atmos. Sci., 72, 2429-2445, 2015.

696 LeMone, M. A., and Zipser, E. J.: Cumulonimbus vertical velocity events in GATE. Part I:
697 Diameter, intensity and mass flux. J. Atmos. Sci., 37, 2444–2457, 1980.

698 Leon, D., and co-authors: The COnvective Precipitation Experiment (COPE): Investigating the
699 origins of heavy precipitation in the southwestern UK. Bull. Amer. Meteor. Soc.
700 doi:10.1175/BAMS-D-14-00157.1, in press, 2016.

701 Lu, C., Liu, Y., Zhang, G. J., Wu, X., Endo, S., Cao, L., Li, Y. and Guo, X.: Improving
702 parameterization of entrainment rate for shallow convection with aircraft measurements and
703 large eddy simulation. J. Atmos. Sci., 2015.

704 Lucas, C., Zipser, E. J., and Lemone, M. A.: Vertical Velocity in Oceanic Convection off
705 Tropical Australia. J. Atmos. Sci., 51, 3183–3193, 1994.

706 May, P. T. and Rajopadhyaya, D. K.: Vertical Velocity Characteristics of Deep Convection over
707 Darwin, Australia. Mon. Wea. Rev., 127, 1056–1071, 1999.

708 Nicol, J. C., Hogan, R. J., Stein, T. H. M., Hanley, K. E., Clark, P. A., Halliwell, C. E., Lean, H.
709 W., and Plant, R. S.: Convective updraught evaluation in high-resolution NWP simulations using
710 single-Doppler radar measurements. Q. J. R. Meteorol. Soc., 141, 3177–3189, 2015.

711 Schmeter, S. M.: Structure of fields of meteorological elements in a cumulonimbus zone, Hydro.
712 Meteor. Serv., Trans. Cent. Aerol. Obs. [Trans. From Russian by Israel Prog. For Sci. Trans.,
713 Jerusalem, 1970, 117 pp.], 1969.

714 Schumacher, C., Stevenson, S. N., and Williams, C. R.: Vertical motions of the tropical
715 convective cloud spectrum over Darwin, Australia. Q.J.R. Meteorol. Soc.. doi: 10.1002/qj.2520,
716 2015.

717 Tiedtke, M.: A comprehensive mass flux scheme for cumulus parameterization in large-scale
718 models. Monthly Weather Review, 117(8), 1779-1800, 1989.

719 Tonttila, J., O'Connor, E. J., Niemelä, S., Räisänen, P., and Järvinen, H.: Cloud base vertical
720 velocity statistics: a comparison between an atmospheric mesoscale model and remote sensing
721 observations. Atmos. Chem. Phys., 11, 9207-9218, 2011.

722 Wang, X., and Zhang M.: Vertical velocity in shallow convection for different plume types, J.
723 Adv. Model. Earth Syst., 6, 478–489, 2014.

724 Wang, Y. and Geerts, B.: Composite Vertical Structure of Vertical Velocity in Nonprecipitating
725 Cumulus Clouds. Mon. Wea. Rev., 141, 1673–1692, 2013.

726 Wang, Z. and co-authors: Single aircraft integration of remote sensing and in situ sampling for
727 the study of cloud microphysics and dynamics. Bull. Amer. Meteor. Soc., 93, 653–668, 2012.

728 Weisman, M. L. and Klemp, J. B.: The dependence of numerically simulated convective storms
729 on vertical wind shear and buoyancy. Monthly Weather Review, 110, 504-520, 1982.

730 Wendisch, M., and Brenguier, J.: Airborne Measurements for Environmental Research: Methods
731 and Instruments. Wiley, 520 pages, 2013.

Wu, J., Del Genio, A. D., Yao, M.-S., and Wolf, A. B.: WRF and GISS SCM simulations of convective updraft properties during TWP-ICE, J. Geophys. Res., 114, D04206, doi:10.1029/2008JD010851, 2009.

Yang, J., Wang, Z., Heymsfield, A. J., and Luo, T.: Liquid/Ice Mass Partition in Tropical Maritime Convective Clouds. J. Atmos. Sci., in review, 2016.

Zipser, E. J., Cecil, D. J., Liu, C., Nesbitt, S. W., and Yorty, D. P.: Where are the most intense thunderstorms on Earth?. Bull. Amer. Meteor. Soc., 87, 1057–1071, 2006.

Table 1. Number of penetrations, time in clouds and flight length in clouds sampled at 0–2 km, 2–4 km, 4–6 km, 6–8 km and 8–10 km MSL in HiCu, COPE and ICE-T.

Height (km MSL)	HiCu			COPE			ICE-T		
	Number of penetrations	Time in clouds (min)	Length in clouds (km)	Number of penetrations	Time in clouds (min)	Length in clouds (km)	Number of penetrations	Time in clouds (min)	Length in clouds (km)
8–10	43	12	79						
6–8	565	122	789				132	52	423
4–6	596	104	653	207	39	244	299	116	895
2–4	373	50	274	378	86	486	34	10	73
0–2				219	40	211	197	27	167

Table 2. Number of updrafts and downdrafts sampled at 0-2 km, 2-4 km, 4-6 km, 6-8 km and 8-10 km in HiCu, COPE and ICE-T. Three numbers are given for the updraft and downdraft at each level, respectively, according to the three different definitions: weak, moderate and strong.

Height (km)		HiCu		COPE		ICE-T	
		Updraft	Downdraft	Updraft	Downdraft	Updraft	Downdraft
8-10	weak	66	100				
	moderate	52	44				
	strong	44	17				
6-8	weak	818	763			382	372
	moderate	559	540			175	136
	strong	287	130			102	23
4-6	weak	748	668	290	184	858	671
	moderate	522	389	232	193	425	329
	strong	343	48	135	51	266	73
2-4	weak	311	235	568	424	49	47
	moderate	271	84	467	434	51	51
	strong	149	7	188	101	32	10
0-2	weak			368	192	319	205
	moderate			266	90	234	104
	strong			96	9	60	7

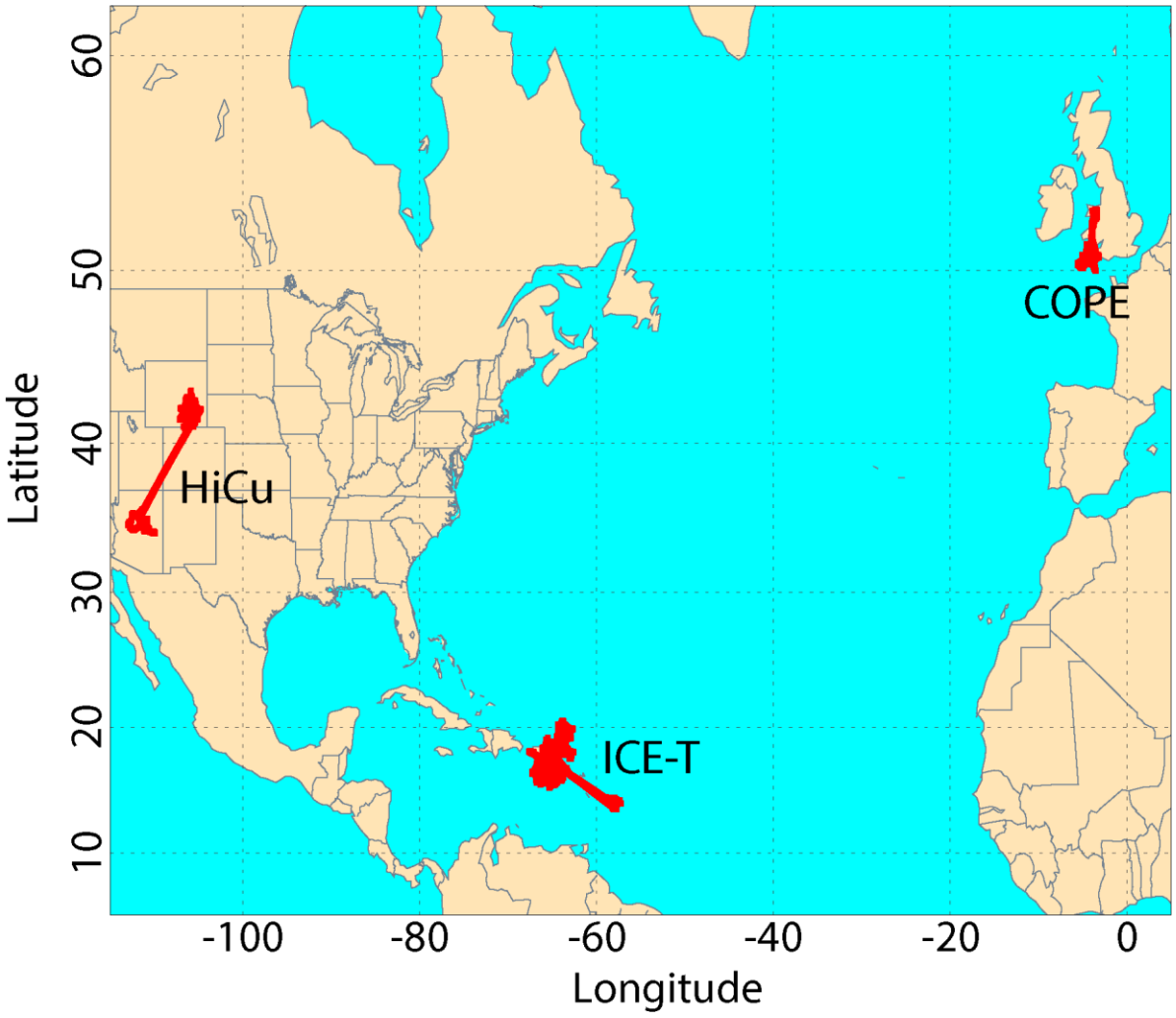

Figure 1. Flight tracks for the three field campaigns: HiCu, COPE and ICE-T.

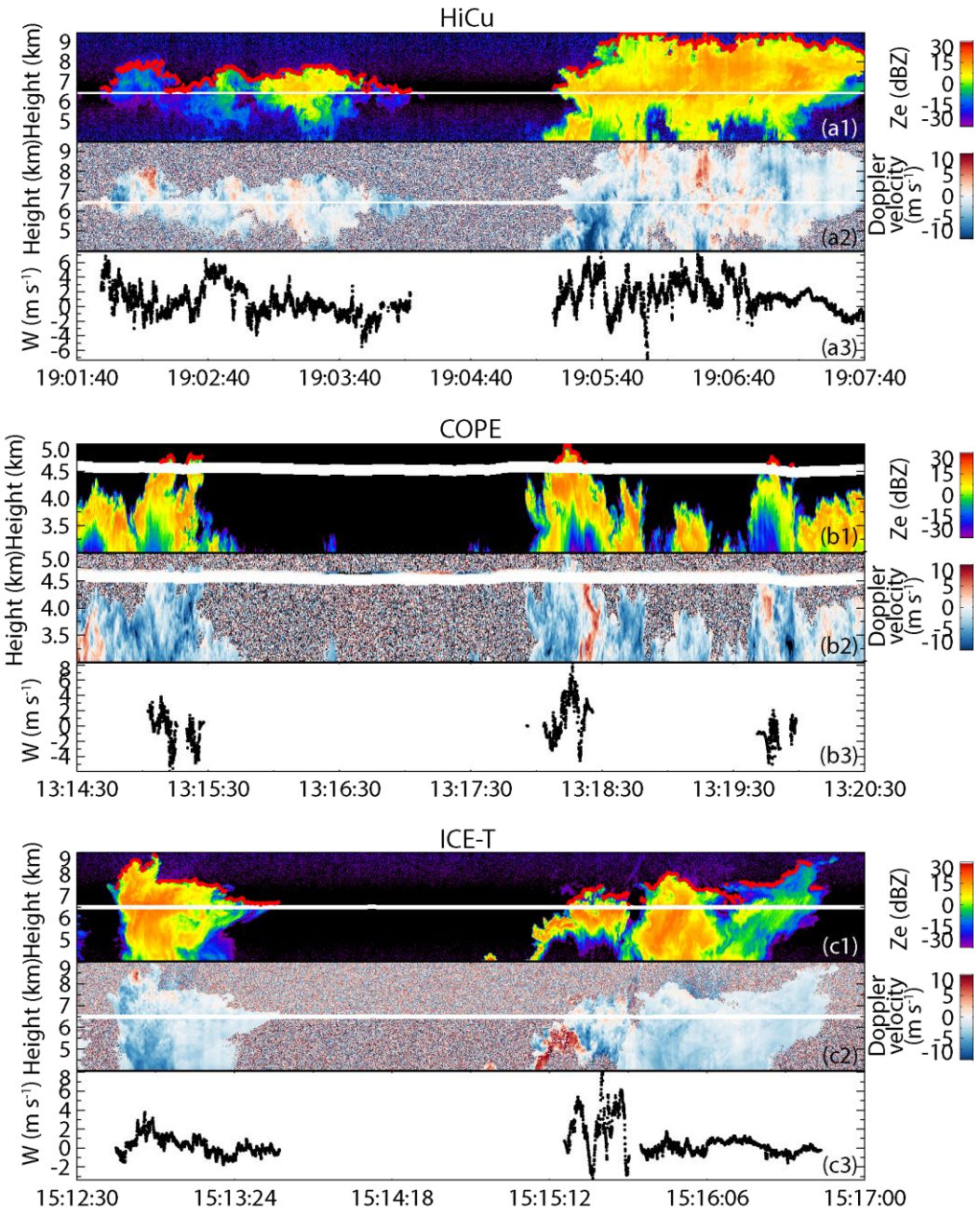

Figure 2. Examples of radar reflectivity, Doppler velocity and 25-Hz in-situ vertical velocity measurements for the convective clouds sampled in HiCu, COPE and ICE-T. The red dots in (a1), (b1) and (c1) are the cloud tops estimated by WCR.

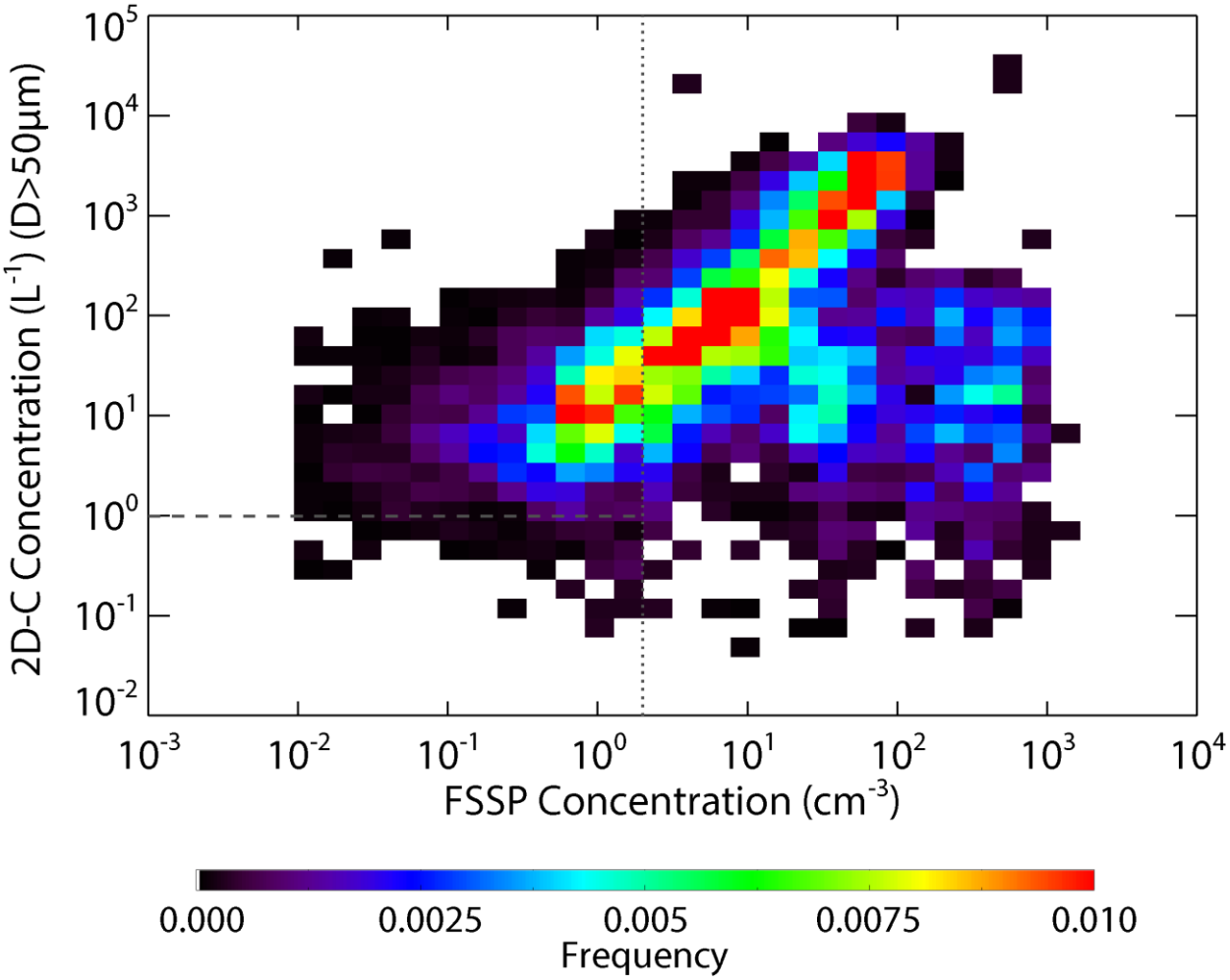

Figure 3. Occurrence distributions as a function of the particle concentrations measured by FSSP versus the concentrations of the particles ≥ 50 μm in diameter measured by 2D-C in the clouds identified by WCR reflectivity. The dashed and dotted lines indicate the FSSP concentration equal 2 cm^{-3} and the 2D-C concentration equal 1 L^{-1}, respectively.

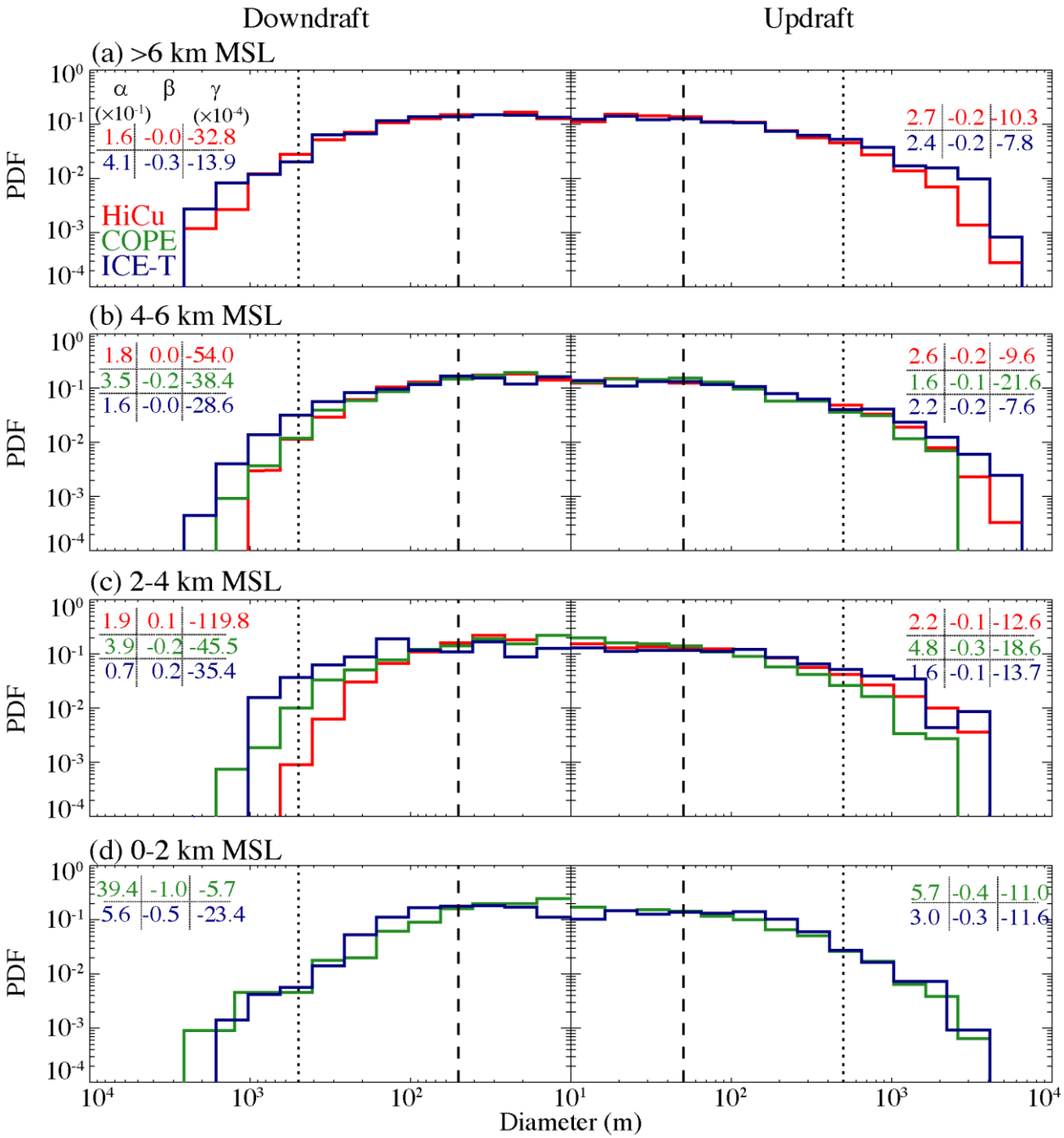

Figure 4. PDFs of the diameters for the updrafts and downdrafts sampled at 0–2 km, 2–4 km, 4–6 km and higher than 6 km. The numbers shown in each panel are the coefficients of the fitted exponential function (Eq. 1).

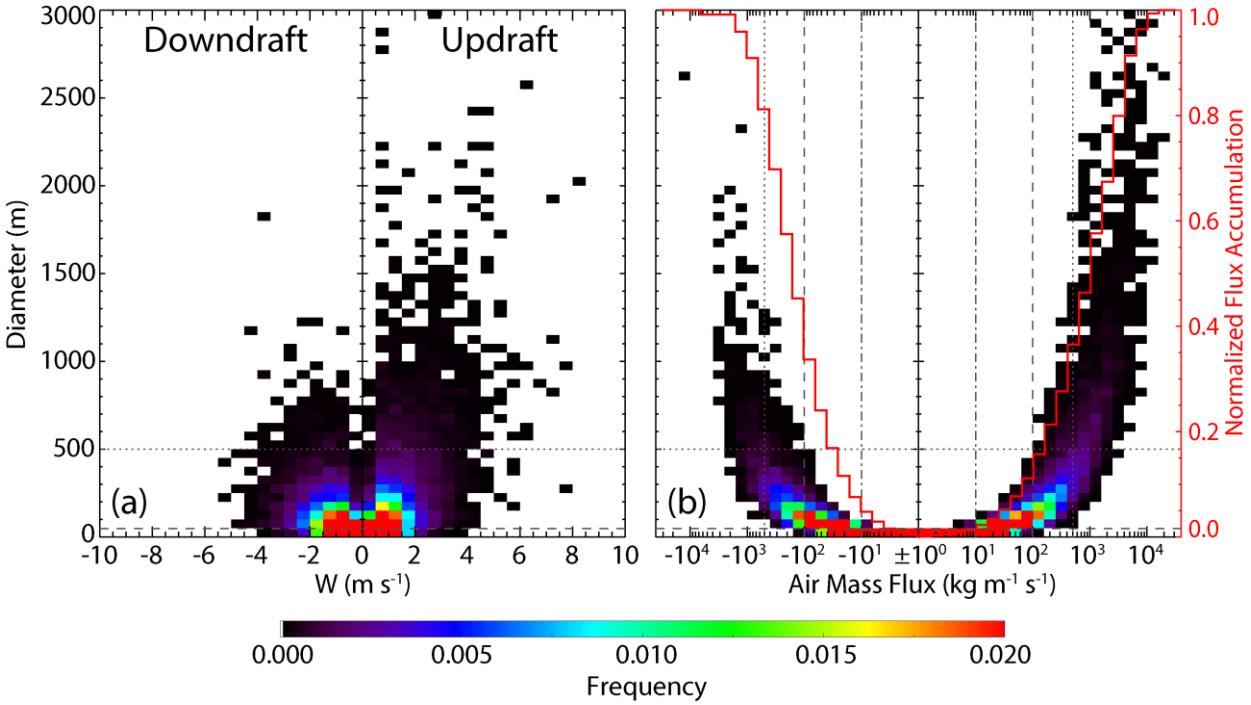

Figure 5. Occurrence distributions as (a) a function of diameter and mean vertical velocity, and (b) a function of diameter and air mass flux for all updrafts and downdrafts. The normalized accumulation flux is also shown by the red curves. The horizontal dotted and dashed lines in (a) and (b) indicate the draft diameter equal 500 m and 50 m, which are used as the diameter thresholds to identify a "draft" in previous studies and in this study, respectively. The vertical dash-dotted, dashed and dotted lines in (b) indicate air mass flux equal 10 kg m^{-1} s^{-1}, 100 kg m^{-1} s^{-1} and 500 kg m^{-1} s^{-1} in magnitude, respectively, which are the thresholds used to delineate the three different groups of draft.

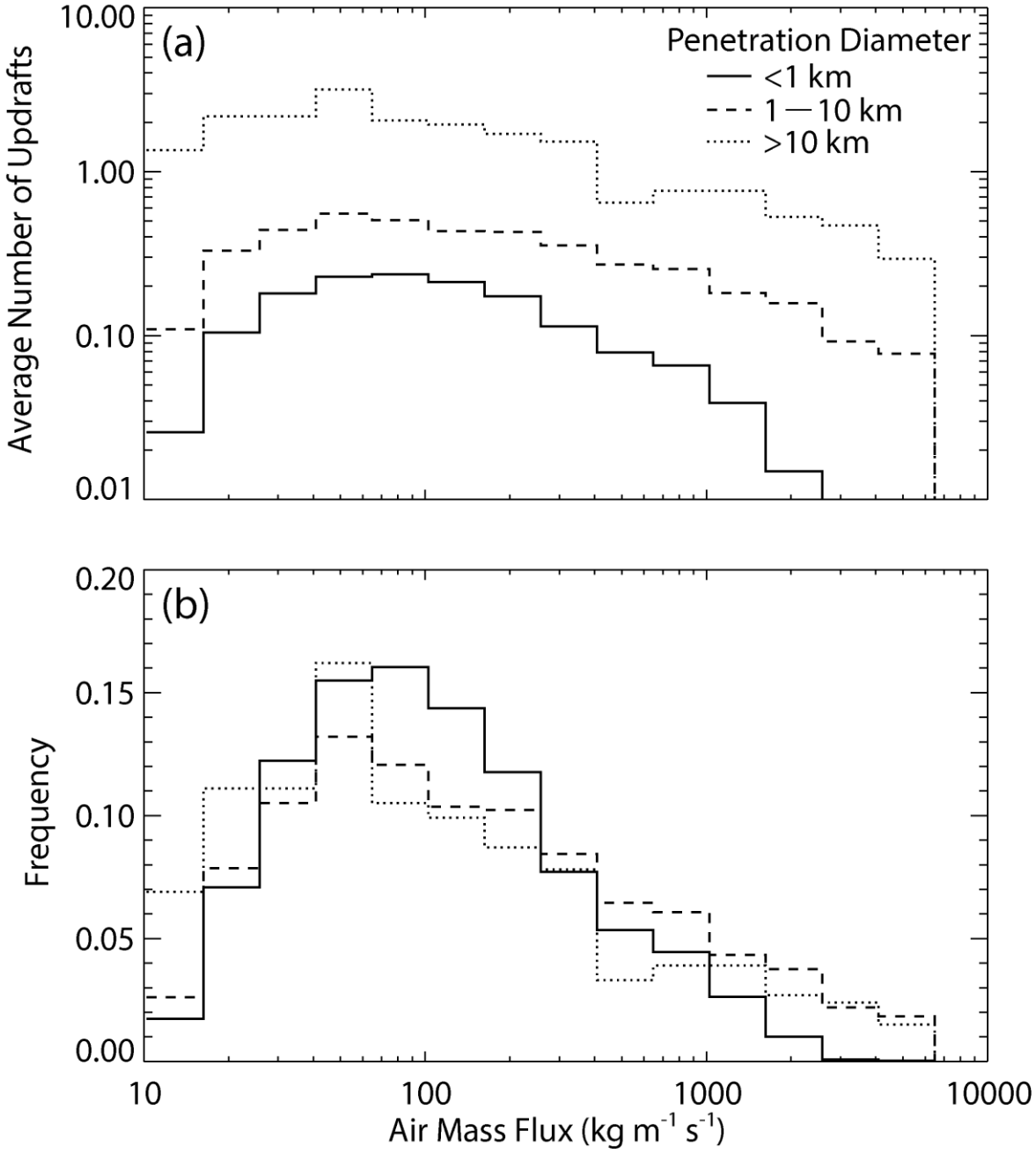

Figure 6. (a) Average number and (b) occurrence frequency of updrafts as a function of air mass flux observed in penetrations with length < 1 km (solid), 1-10 km (dashed) and >10 km (dotted). The result is a composite of HiCu, COPE and ICE-T.

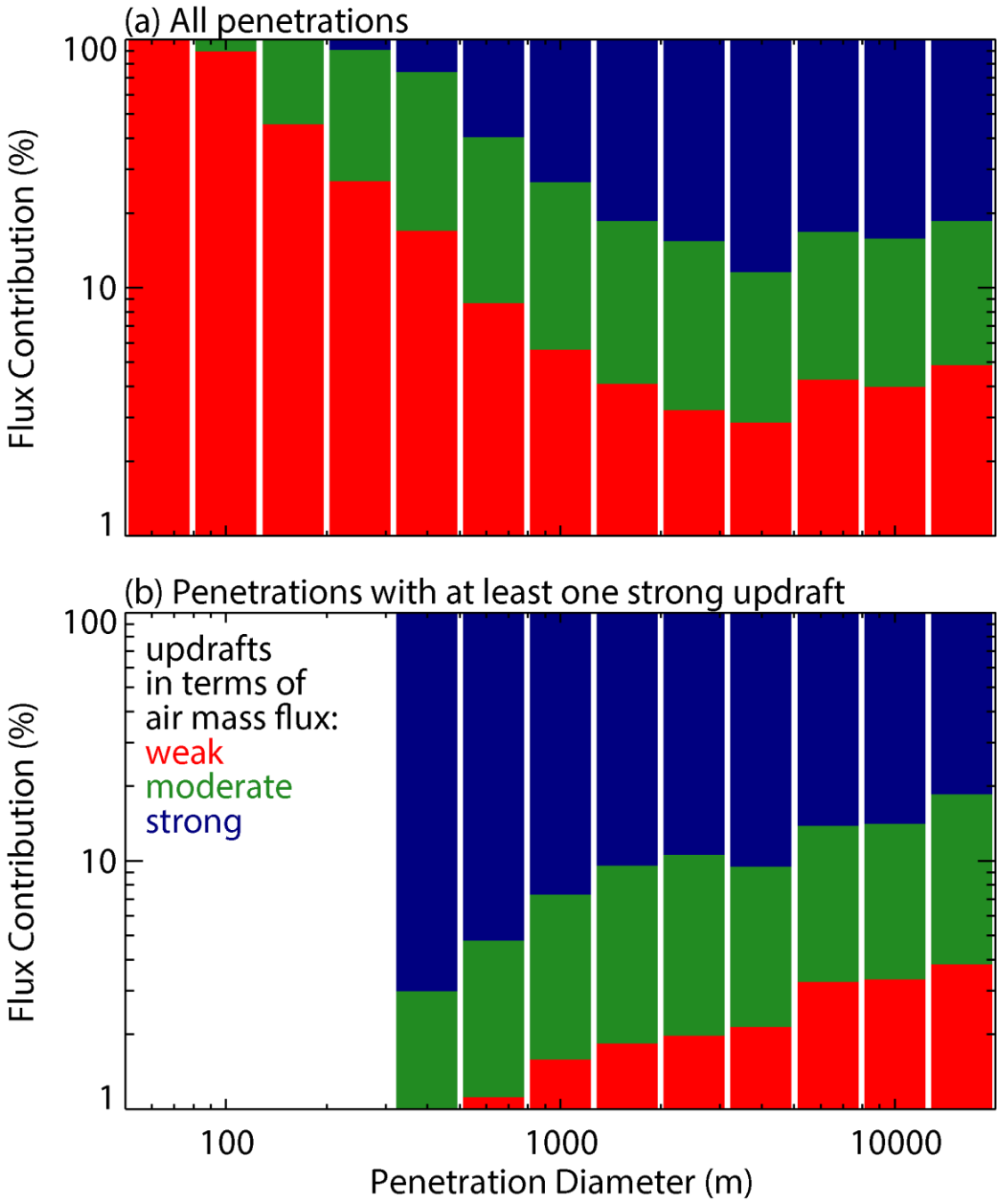

Figure 7. Average percentile contribution to total upward air mass flux by the weak (red), moderate (green) and strong (blue) updrafts delineated in this study. The result is a composite of HiCu, COPE and ICE-T.

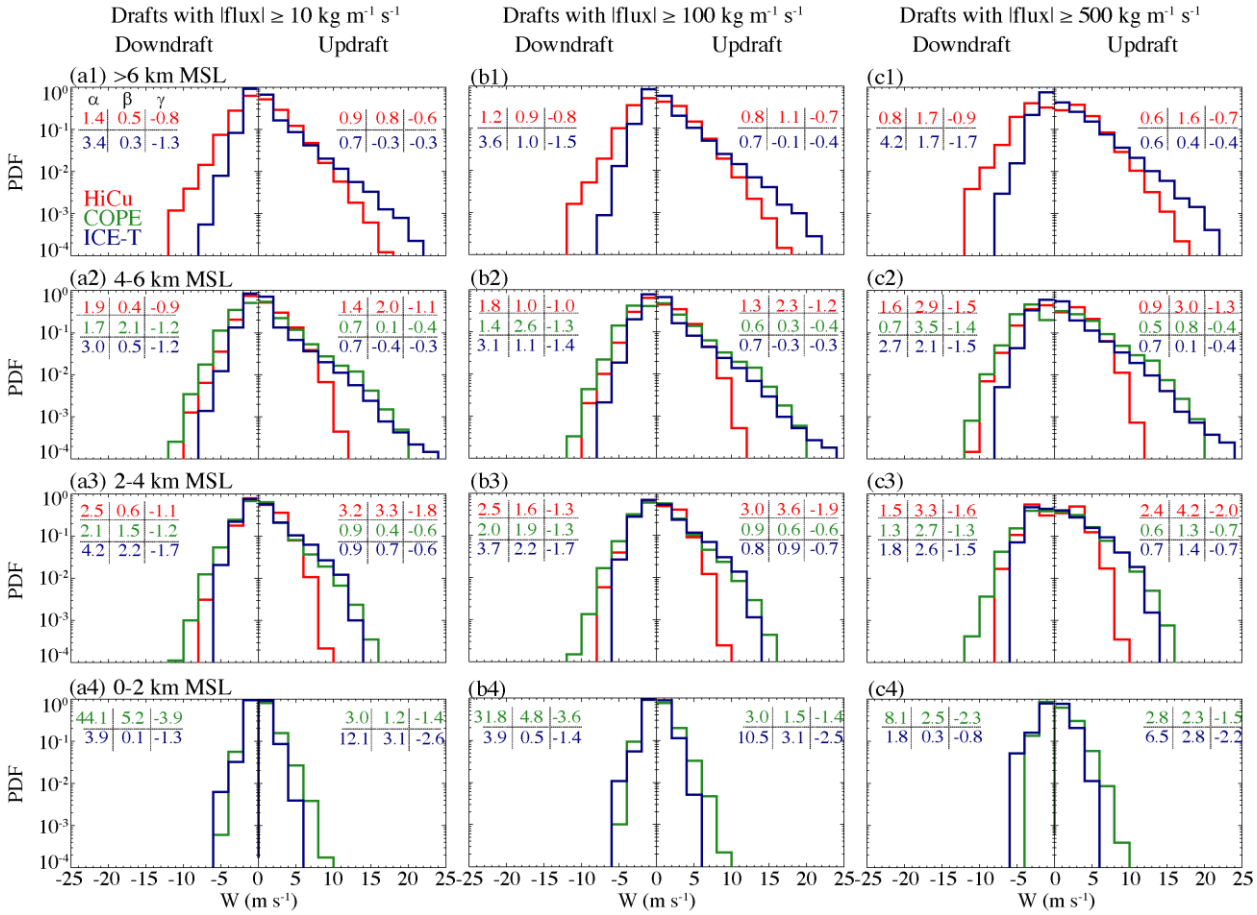

Figure 8. PDFs of the 25-Hz vertical velocity for the updrafts and downdrafts with air mass flux ≥ (a) 10 kg m^{-1} s^{-1}, (b) 100 kg m^{-1} s^{-1} and (c) 500 kg m^{-1} s^{-1} in magnitude, sampled at 0–2 km, 2–4 km, 4–6 km and higher than 6 km. The numbers shown in each panel are the coefficients of the fitted exponential function (Eq. 1).

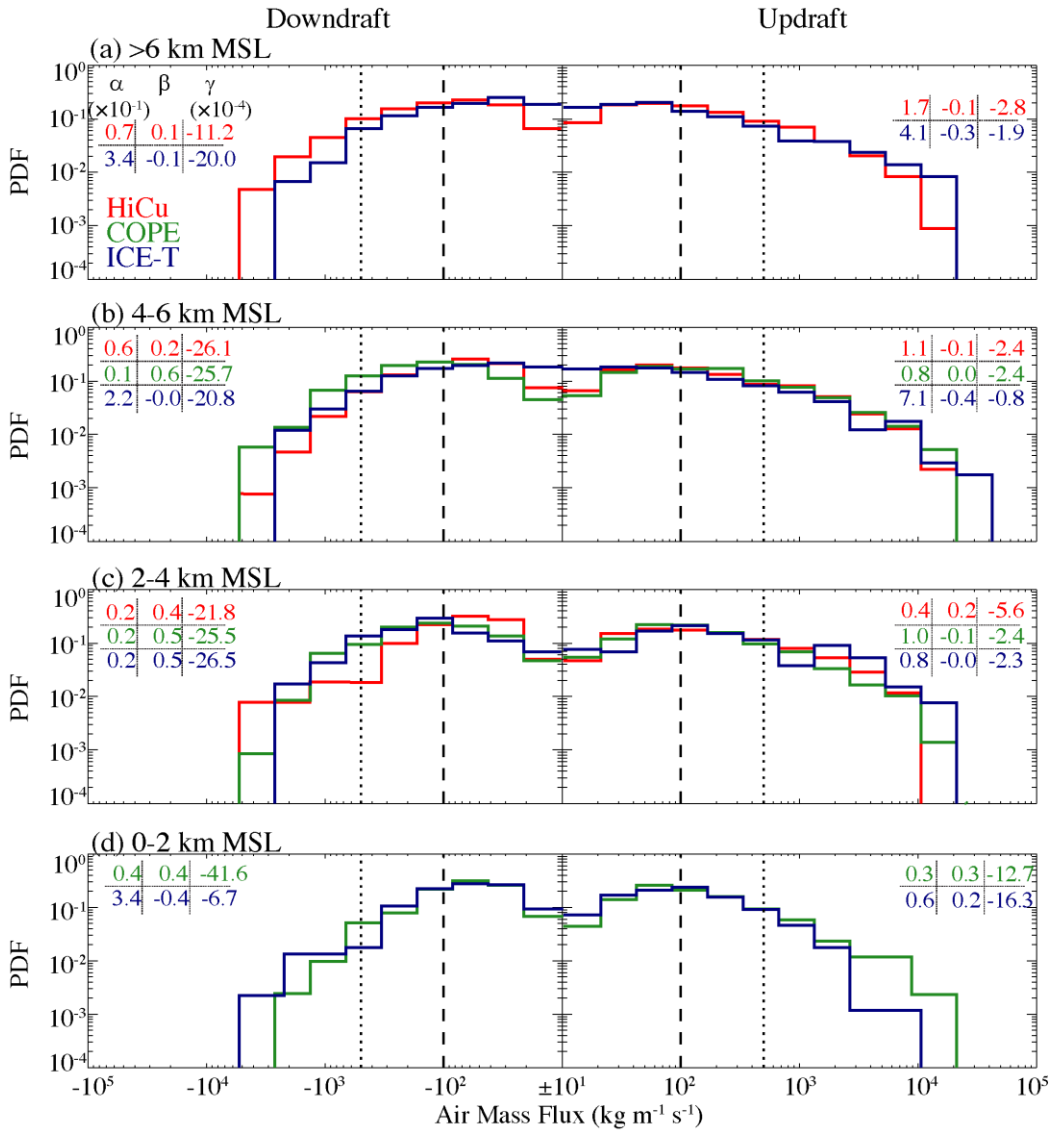

Figure 9. PDFs of the air mass flux for the updrafts and downdrafts sampled at 0–2 km, 2–4 km, 4–6 km and higher than 6 km. The three thresholds of the air mass flux (±10 kg m^{-1} s^{-1}, ±100 kg m^{-1} s^{-1} and ±500 kg m^{-1} s^{-1}) are shown by the solid (overlaps with the central y-axis in each panel), dashed and dotted lines. The numbers shown in each panel are the coefficients of the fitted exponential function (Eq. 1).

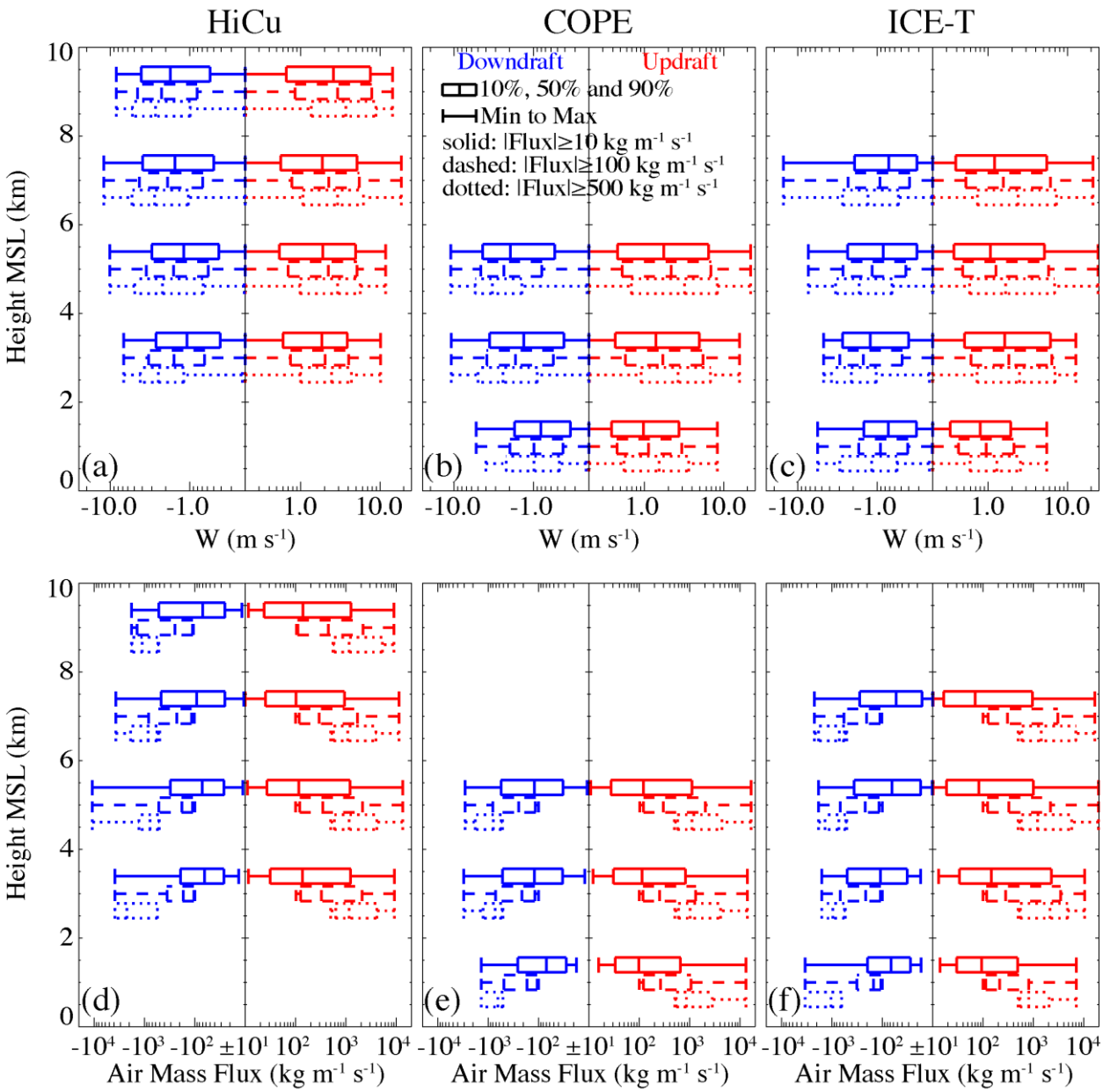

Figure 10. Profiles of (a-c) the vertical velocity and (d-f) air mass flux for all the updrafts and downdrafts sampled at 0–2 km, 2–4 km, 4–6 km, 6–8 km and 8–10 km. The dotted, dashed and solid boxes represent for the drafts with air mass flux ≥ 10 kg m^{-1} s^{-1}, 100 kg m^{-1} s^{-1} and 500 kg m^{-1} s^{-1} in magnitude, respectively.

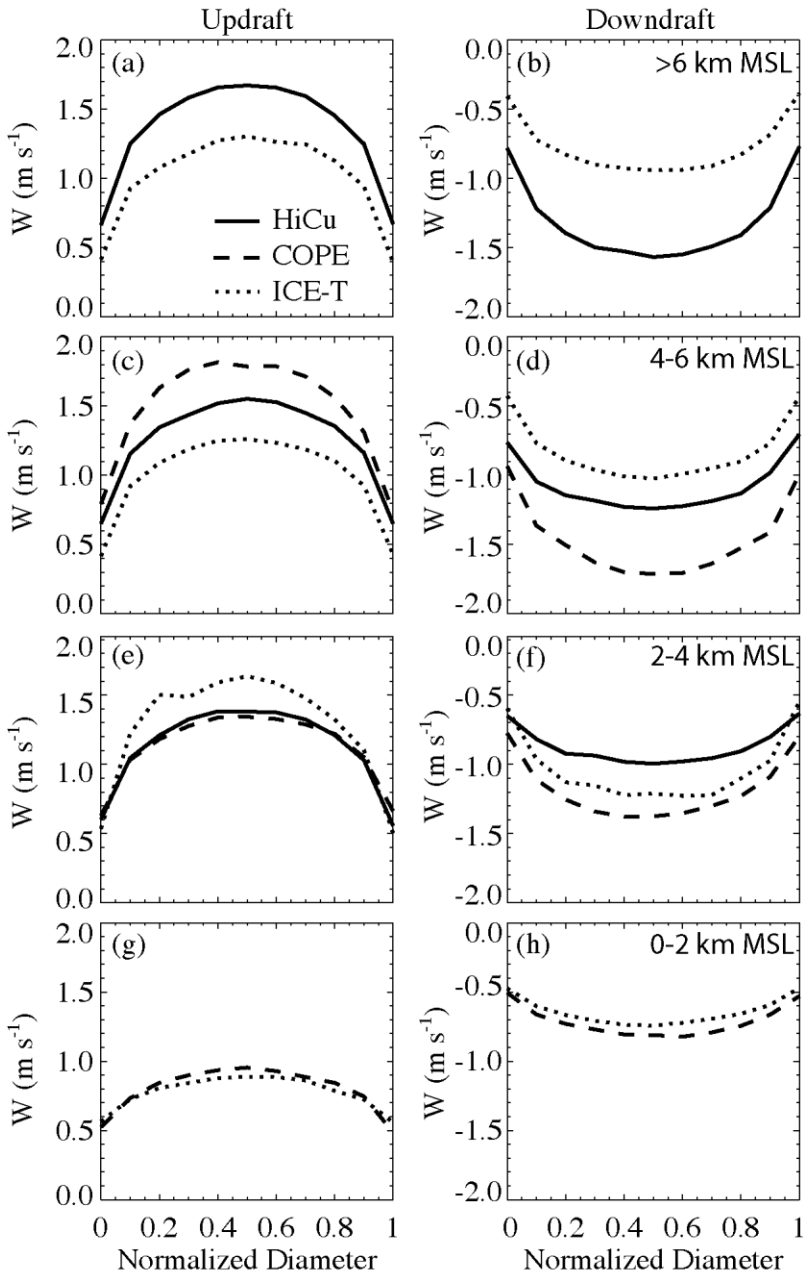

Figure 11. Composite structure of the vertical velocity as a function of the normalized diameter for the updrafts and downdrafts with air mass flux ≥ 10 kg m^{-1} s^{-1} in magnitude. The 0 and 1 coordinates on the x-axis indicate the upwind and downwind sides of the draft.

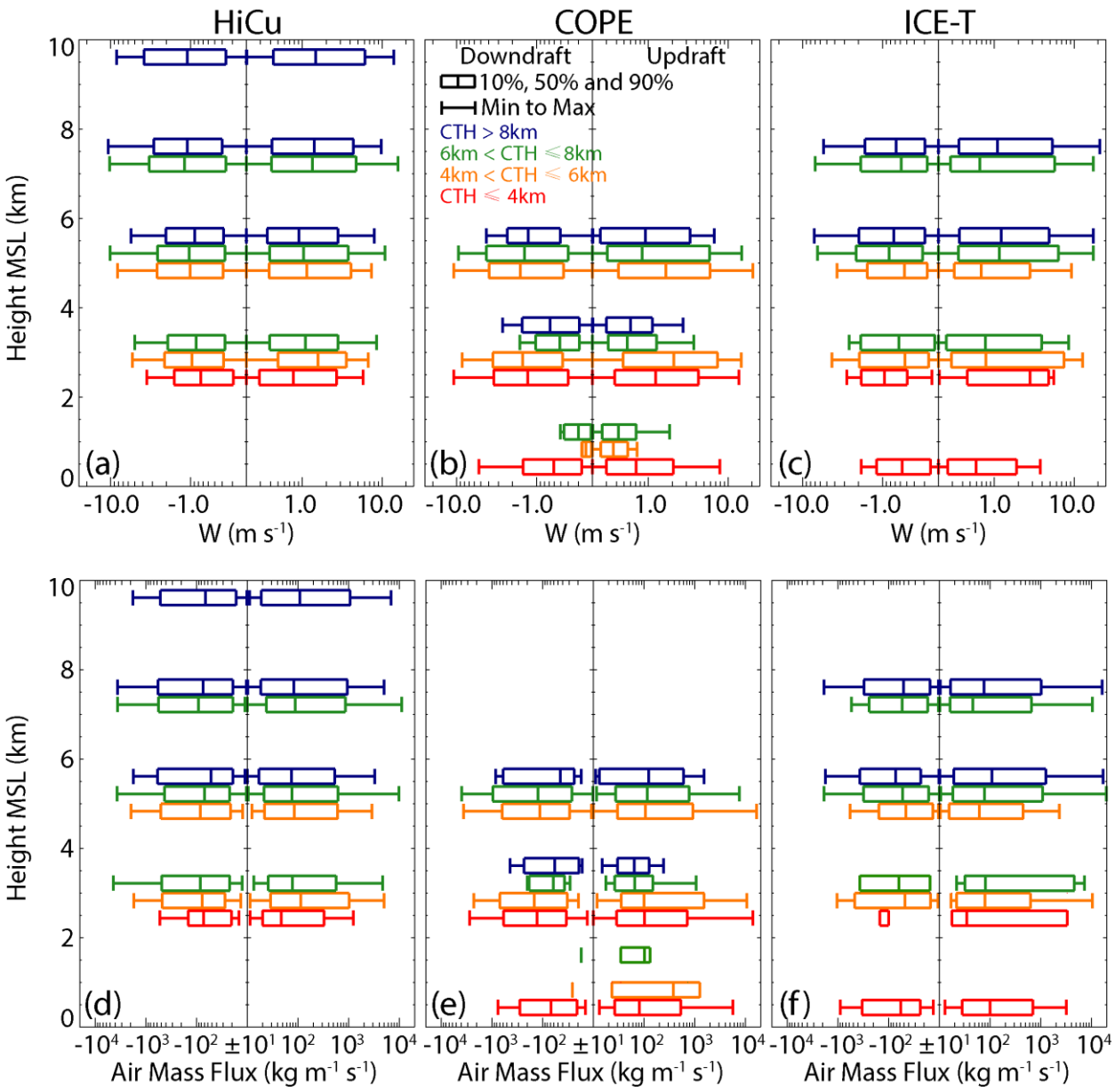

Figure 12. Profiles of (a-c) the vertical velocity and (d-f) the air mass flux for the updraft and downdraft with air mass flux ≥ 10 kg m^{-1} s^{-1} in magnitude. The red, orange, green and blue boxes represent clouds with cloud top heights of 0-4 km, 4-6 km, 6-8 km and higher than 8 km.